# Title: Cyclodextrin promotes atherosclerosis regression via macrophage reprogramming

**Authors:**

Sebastian Zimmer[1†], Alena Grebe[2†], Siril S. Bakke[2,3,4], Niklas Bode[1], Bente Halvorsen[5], Thomas Ulas[6], Mona Skjelland[7], Dominic De Nardo[2,8,9], Larisa I. Labzin[2], Anja Kerksiek[10], Chris Hempel[11], Michael T. Heneka[12], Victoria Hawxhurst[13], Michael L Fitzgerald[13], Jonel Trebicka[14, 15], Ingemar Björkhem[16], Jan-Åke Gustafsson[17], Marit Westerterp[18], Alan R. Tall[18], Samuel D. Wright[19], Terje Espevik[4], Joachim L. Schultze[3,6], Georg Nickenig[1], Dieter Lütjohann[10] and Eicke Latz[2,3,4,20]*

**Affiliations:**

[1] Medizinische Klinik und Poliklinik II, University Hospitals Bonn, 53105 Bonn, Germany
[2] Institute of Innate Immunity, University Hospitals Bonn, 53127 Bonn, Germany
[3] German Center of Neurodegenerative Diseases (DZNE), 53127 Bonn, Germany
[4] Centre of Molecular Inflammation Research at the Norwegian University of Science and Technology, 7489 Trondheim, Norway
[5] Research Institute of Internal Medicine, Oslo University Hospital Rikshospitalet, Norway; Institute of Clinical Medicine and K.G. Jebsen Inflammatory Research Center, University of Oslo, 0424 Oslo, Norway
[6] Genomics and Immunoregulation, Life and Medical Sciences Institute, University of Bonn, 53115 Bonn, Germany
[7] Department of Neurology, Oslo University Hospital and University of Oslo, Oslo, Norway.
[8] Inflammation Division, The Walter and Eliza Hall Institute of Medical Research, Parkville Victoria 3052, Australia
[9] Department of Medical Biology, The University of Melbourne, Parkville 3010, Australia
[10] Institute of Clinical Chemistry und Clinical Pharmacology, University Hospitals Bonn, 53105 Bonn, Germany
[11] Addi and Cassi Fund, Reno, NV 89511, USA
[12] Clinic and Polyclinic for Neurology, University Hospitals Bonn, 53105 Bonn, Germany
[13] Lipid Metabolism Unit, Center for Computational and Integrative Biology, Boston, MA 02114, USA
[14] Medizinische Klinik und Poliklinik I, University Hospitals Bonn, 53105 Bonn, Germany
[15] Faculty of Health Sciences University of Southern Denmark Campusvej 55, DK-5230 Odense M, Denmark
[16] Division of Clinical Chemistry, Karolinska Institutet, Huddinge University Hospital, 141 86 Huddinge, Sweden
[17] Center for Nuclear Receptors and Cell Signaling, University of Houston, Houston, TX 77004, USA
[18] Department of Medicine, Columbia University, New York, NY 10032, USA
[19] CSL Behring, King of Prussia, PA 19406, USA
[20] Department of Infectious Diseases and Immunology, UMass Medical School, Worcester, MA 01605, USA

* To whom correspondence should be addressed: Eicke Latz, MD, PhD, Institute of Innate Immunity, University Hospitals Bonn, Sigmund-Freud-Str. 25, 53127 Bonn, Germany, e-mail: eicke.latz@uni-bonn.de, phone: +49 228 287 51223

† equal contribution

**Abstract**: Atherosclerosis is an inflammatory disease linked to elevated blood cholesterol concentrations. Despite ongoing advances in the prevention and treatment of atherosclerosis, cardiovascular disease remains the leading cause of death worldwide. Continuous retention of apolipoprotein B-containing lipoproteins in the subendothelial space causes a local overabundance of free cholesterol. Because cholesterol accumulation and deposition of cholesterol crystals (CCs) triggers a complex inflammatory response, we tested the efficacy of the cyclic oligosaccharide 2-hydroxypropyl-β-cyclodextrin (CD), a compound that increases cholesterol solubility, in preventing and reversing atherosclerosis. Here we show that CD treatment of murine atherosclerosis reduced atherosclerotic plaque size and CC load, and promoted plaque regression even with a continued cholesterol-rich diet. Mechanistically, CD increased oxysterol production in both macrophages and human atherosclerotic plaques, and promoted liver X receptor (LXR)-mediated transcriptional reprogramming to improve cholesterol efflux and exert anti-inflammatory effects. *In vivo*, this CD-mediated LXR agonism was required for the anti-atherosclerotic and anti-inflammatory effects of CD as well as for augmented reverse cholesterol transport. Because CD treatment in humans is safe and CD beneficially affects key mechanisms of atherogenesis, it may therefore be used clinically to prevent or treat human atherosclerosis.

**One Sentence Summary:** The cyclic oligosaccharide 2-hydroxypropyl-β-cyclodextrin facilitates atheroprotective mechanisms through oxysterol-mediated reprogramming of macrophages.

## Introduction

Atherosclerosis is the underlying pathology that causes heart attacks, stroke, and peripheral vascular disease. Collectively, these conditions represent a common health problem, and current treatments are insufficient to adequately reduce the risk of disease development. Pharmacologic reduction *(1-3)* of high cholesterol concentrations is among the most successful therapeutic approaches to reduce the risk of developing cardiovascular disease and stroke, but adequate reduction of low-density lipoprotein cholesterol is not possible in all patients.

Atherosclerosis is characterized by arterial wall remodeling, which is initiated by the retention and accumulation of different classes of lipids in the subendothelial layer. Lipid deposition and the appearance of cholesterol crystals (CCs) has been associated with the induction of an inflammatory reaction in the vessel wall, which contributes to the pathogenesis *(4, 5)*. Indeed, patients with increased systemic inflammation have increased risk of cardiovascular death, and studies are underway to test whether anti-inflammatory treatment can reduce cardiovascular event rates *(6)*.

CCs, which can result from excessive cholesterol deposition in atherosclerotic lesions, are among the proinflammatory triggers that contribute to the inflammatory response during atherogenesis *(7)*. CCs can trigger complement activation and neutrophil extracellular trap (NET) formation, as well as induction of innate immune pathways *(4, 5, 8-10)*. Hence, therapeutic strategies aimed at

the prevention of cholesterol phase transition or the removal of CCs could reduce tissue inflammation and disease progression.

Genetic approaches to increase the capacity of macrophages to remove free cholesterol from atherosclerotic lesions have proven to be highly successful in preclinical trials *(11)*. This prompted us to test whether pharmacologically increasing cholesterol solubility, clearance, and catabolism can be exploited for the prevention or treatment of atherosclerosis. 2-hydroxypropyl-β-cyclodextrin (CD) is an FDA-approved substance used to solubilize and entrap numerous lipophilic pharmaceutical agents for therapeutic delivery in humans *(12, 13)*. Although it has previously been shown that CD increases cholesterol solubility, promotes the removal of cholesterol from foam cells *in vitro,* and initiates anti-inflammatory mechanisms *(14-16)*, it remains unknown whether CD can exert anti-atherogenic effects *in vivo*.

Here, we found that subcutaneous administration of CD profoundly reduced atherogenesis and induced regression of established atherosclerosis in mouse models. CD augmented dissolution of CCs, reducing their appearance in lesions. Furthermore, CD increased cholesterol metabolism and liver X receptor (LXR)-dependent cellular reprogramming, which resulted in more efficient reverse cholesterol transport (RCT) as well as reduced pro-inflammatory gene expression. The atheroprotective effect of CD was dependent on LXR expression in myeloid cells transplanted into LDLR-deficient mice. These studies suggest that CD mediates atheroprotection by increasing production of oxysterols and LXR-dependent cellular reprogramming and provide preclinical evidence that CD could be developed into an effective therapy for atherosclerosis in humans.

## Results

*Cyclodextrin treatment impairs atherogenesis.*

To investigate the efficacy of CD treatment in murine atherosclerosis, $ApoE^{-/-}$ mice were fed a cholesterol-rich diet and concomitantly treated subcutaneously with CD or vehicle control for eight weeks. Although plasma cholesterol, the main driver of atherosclerosis, remained unaffected (Fig. 1A), CD treatment profoundly reduced atherosclerotic lesions within the aortic root (Fig. 1B). Furthermore, we found reduced amounts of CCs in atherosclerotic plaques of CD treated mice as assessed by laser reflection microscopy (Fig. 1C, D). CD did not influence weight gain, blood pressure, heart rate, or the number of bone marrow-derived or circulating sca1/flk1 positive cells (Fig. S1A-E). Moreover, plasma concentrations of phytosterols, cholestanol, and cholesterol precursors were not influenced by CD treatment, indirectly showing that CD did not alter cholesterol enteric uptake or overall endogenous biosynthesis (Fig. S1F) *(17)*. CD also did not change the relative plaque composition, including cellularity and macrophage content (Fig. 1E, F). However, production of aortic reactive oxygen species (Fig. 1G) and plasma concentrations of pro-inflammatory cytokines were reduced by CD treatment (Fig. 1H-J), suggesting that CD may reduce the inflammatory response during atherogenesis.

*Cyclodextrin treatment mediates regression of atherosclerotic plaques.*

Although continuous drug administration in parallel to Western diet feeding of mice is a standard protocol to investigate potential atheroprotective substances *(18)*, patients are generally not treated in early stages of atherogenesis. Therefore, we tested the effect of CD treatment on atherosclerosis regression. $ApoE^{-/-}$ mice are hypercholesterolemic even on normal or lipid-reduced chow, and thus most murine atherosclerotic regression models rely on interventional

strategies that normalize plasma lipids, such as viral gene transfer, transplantation, or infusion of high-density lipoprotein (HDL) particles *(19)*. We adapted a less invasive regression protocol *(20)*, in which ApoE$^{-/-}$ mice were first fed a cholesterol-rich diet for eight weeks to induce advanced atherosclerotic lesions, and then switched to a normal chow diet for another four weeks, during which CD or vehicle control was administered (Fig. 2A). As expected, plasma cholesterol concentrations were decreased in both groups compared to baseline, but no difference between control and CD treatment was observed (Fig. 2B, Fig. S2A). Although switching to a normal chow diet had no effect on atherosclerotic lesion size in vehicle treated mice, CD treatment resulted in a regression of atherosclerotic plaques by approximately 45% (Fig. 2C). Although CC load in lesions was already decreased in vehicle treated animals compared to the load before treatment, CC amounts were further reduced by CD treatment (Fig. 2D). Because patients with cardiovascular disease often do not adhere to the recommended lifestyle changes, which include dietary modifications, we next investigated whether CD treatment can affect atherosclerosis regression during continuous enteric cholesterol challenge. CD or vehicle treatment was started after eight weeks of cholesterol-rich diet, which was continued for the entire 12 weeks (Fig. 2E). Although plasma cholesterol and general cholesterol metabolism were not altered (Fig. 2F, Fig. S2B), atherosclerotic plaque size and CC load were decreased in CD treated mice on continuous cholesterol-rich diet (Fig. 2G, H). These data demonstrate that CD treatment is effective in reducing established plaques.

*Cyclodextrin dissolves extra- and intracellular cholesterol crystals.*

There are several possibilities to explain the protective effects of CD treatment on both atherogenesis and established atherosclerosis. Because CD is known to form soluble inclusion complexes with cholesterol, thereby enhancing its solubility in aqueous solutions by approximately 150,000-fold, we tested whether CD increases the solubility of CCs. Indeed, fluorescent CD bound to the surface of CCs (Fig. 3A, B), and CD mediated the solubilization of CCs in a dose-dependent manner (Fig. 3C). To be effective in atherosclerotic plaques, CD must also act on intracellular CCs. Indeed, macrophages rapidly internalized fluorescent CD (Fig. 3D) and concentrated it in intracellular compartments (Fig. 3E). Furthermore, incubation with 10 mM CD, a subtoxic dose (Fig. S3), enhanced the dissolution of intracellular CCs over time (Fig. 3F, Fig. S4).

*Metabolism of crystal-derived cholesterol is increased by cyclodextrin.*

Macrophages within the arterial wall take up excessive amounts of cholesterol and transform into foam cells, a process that can impair macrophage function and promote atherogenesis *(21)*. This can be mimicked *in vitro* by loading macrophages with CCs (Fig. S5). After uptake of CCs into phagosomes, cholesterol is moved from the lysosome via the Niemann-Pick C1 (NPC1) transporter to the endoplasmic reticulum, where acetyl-CoA acetyltransferase catalyzes the formation of cholesteryl esters. This mechanism turns excess free cholesterol, which forms crystals and is cytotoxic, into cholesteryl esters that can be stored in lipid droplets. A second pathway to metabolize free cholesterol is the formation of water-soluble oxysterols. Oxysterols can diffuse across cell membranes and are known to reprogram macrophages via activation of LXR, which in turn modulates the inflammatory response and supports RCT to HDL *(22-24)*. To study how CD influences the ability of macrophages to reduce the amount of cholesterol derived from CCs, we incubated macrophages with CCs prepared from $D_6$-cholesterol ($D_6$-CCs) and followed $D_6$-cholesterol metabolism products in cells and cellular supernatants by gas chromatography-mass spectrometry selective ion monitoring (GC-MS-SIM) (Fig. 4A). This analysis revealed that CD treatment promoted esterification of crystal-derived $D_6$-cholesterol

(Fig. 4B). Furthermore, CD amplified $D_6$-cholesterol concentrations in supernatants, while reducing the overall cellular pool of $D_6$-cholesterol (Fig. 4C). Hence, CD treatment increased the cholesterol efflux capacity of macrophages, which represents an important protective factor in patients with coronary artery disease *(25, 26)*. Active cholesterol transport is mediated primarily by the ATP-binding cassette transporters A1 and G1 (ABCA1 and ABCG1), which transfer free cholesterol to ApoA1 and mature HDL particles, respectively *(27)*. In line with the observed increase in cholesterol efflux capacity, macrophages incubated with CCs had increased expression of both ABCA1 and ABCG1, which was even further enhanced by CD treatment (Fig. 4D-F). Genes involved in driving cholesterol efflux, including *Abca1* and *Abcg1*, are under control of the liver X receptor/ retinoid X receptor (LXR/RXR) transcription apparatus *(22, 28)*. Because the transcriptional activities of LXRs are positively regulated by oxysterols, we next analyzed whether CD can potentiate cholesterol oxidation. Indeed, we found that CD treatment of $D_6$-CC loaded macrophages resulted in a dramatic 15-fold increase of $D_6$-cholesterol-derived 27-hydroxycholesterol ($D_5$-27-hydroxycholesterol) (Fig. 4G), although the expression of *Cyp27a1* was not altered (Fig. S6). Unexpectedly, CD also increased 27-hydroxycholesterol production and secretion from macrophages under normocholesterolemic conditions, meaning macrophages not treated with $D_6$-CCs (Fig. 4H). Hence, CD increases the metabolism of free cholesterol and could thereby lower the potential for its phase transition into crystals.

*Cyclodextrin induces LXR target gene expression in macrophages.*

The drastic CD-mediated increase of oxysterol production upon $D_6$-CC loading and the unanticipated finding that CD can increase oxysterols in normocholesterolemic macrophages prompted us to comprehensively investigate whether CD influences the expression profiles of LXR-regulated genes. Wild type (WT) or LXR$\alpha^{-/-}\beta^{-/-}$ macrophages were exposed to CD, CC, or CC and CD, and gene expression was assessed by genome-wide mRNA profiling. To investigate whether CD changes LXR target gene expression in macrophages, we performed gene set enrichment analysis (GSEA) *(29)* with a set of 533 of previously identified LXR target genes *(30)* (Fig. 5A and Table S1). Enrichment of LXR target gene sets was identified when WT macrophages were incubated with CCs (Fig. 5B), presumably due to cholesterol overloading of macrophages. Consistent with the strong induction of CC-derived 27-hydroxycholesterol and the observed increase in cholesterol efflux by CD, LXR target gene sets were enriched when CD was added together with CCs (Fig. 5B). CD treatment alone also resulted in LXR gene set enrichment under normocholesterolemic conditions, which correlates with the observed induction of cellular 27-hydroxycholesterol (Fig. 4H). In LXR$\alpha^{-/-}\beta^{-/-}$ macrophages, none of the conditions resulted in significant enrichments of LXR target gene sets (Fig. 5C). Furthermore, these findings could be confirmed for the key LXR target genes ABCA1 and ABCG1 in WT and LXR$\alpha^{-/-}\beta^{-/-}$ macrophages on the mRNA and protein levels (Fig. 5D-F) *(31)*.

*Cyclodextrin increases in vivo reverse cholesterol transport.*

To test whether CD-induced LXR reprogramming of macrophages improves macrophage cholesterol efflux *in vivo*, bone marrow-derived macrophages (BMDM) from WT or LXR$\alpha^{-/-}\beta^{-/-}$ mice were loaded with $D_6$-CCs *ex vivo* and injected into the peritoneum of WT mice. The mice carrying crystal-loaded macrophages were then treated with CD or vehicle control, and $D_6$-cholesterol excretion into the feces and urine was monitored by GC-MS-SIM (Fig. 6A). CD increased RCT of crystal-derived $D_6$-cholesterol from WT, and to a lower extent from LXR$\alpha^{-/-}\beta^{-/-}$ macrophages (Fig. 6B). Of note, CD treatment not only induced $D_6$-cholesterol excretion into the feces but also promoted urinary $D_6$-cholesterol elimination (Fig. 6C), a process that is normally not observed during RCT. Prior work on Niemann-Pick type C disease, a rare genetic disorder in

which cholesterol cannot escape the lysosome, has shown that CD can mobilize lysosomal cholesterol and activate LXR-dependent gene expression *(32, 33)*. NPC1-deficient patients receive weekly injections of CD with the aim of overcoming this cholesterol transport defect (ClinicalTrial.gov NCT01747135). To investigate whether CD can also stimulate urinary cholesterol excretion in humans, we monitored urinary cholesterol excretion of patients with NPC1 mutations after CD infusion over time. Indeed, CD, which is primarily excreted via the urinary tract, resulted in a time-dependent cholesterol excretion into the urine (Fig. 6D). These data suggest that CD enhances *in vivo* RCT from macrophages, partially in an LXR-dependent manner, but can also directly extract and transport cholesterol for excretion.

*Cyclodextrin modifies human plaque cholesterol metabolism and gene expression.*

To test whether the protective functions of CD on murine macrophages are also exerted in human atherosclerotic plaques, we next performed lipid and genomic analyses on biopsy specimens obtained from carotid endarterectomies (Fig. 7A). Comparable to our findings in murine macrophages, incubation of human atherosclerotic plaques with CD resulted in a transfer of cholesterol from plaques to supernatants (Fig. 7B). Moreover, we observed an increase in the production of 27-hydroxycholesterol, which was mainly released into the supernatants of the CD treated plaques (Fig. 7C). Gene expression profiling of a large panel of human immunology-related genes and selected LXR target genes was performed in resting or treated plaque tissue. These gene expression data were analyzed by several bioinformatics approaches. First, we performed gene ontology enrichment analysis (GOEA) using the genes differentially regulated after treatment with CD or vehicle control. Consistent with our lipid results, we found that genes involved in lipid transport, storage, metabolism, and efflux were up-regulated upon CD exposure. Conversely, genes known to regulate immune responses, represented by terms such as 'regulation of immune responses in lymphocytes', 'regulation of leukocyte mediated immunity' or 'interleukin response, T cell and NK cell regulation' were down-regulated after CD treatment (Fig. 7D). Further interrogation of the GOEA revealed that CD treatment of human plaques affected many key genes in the GO term "regulation of inflammatory response" (GO:0050727). These included innate immune receptors, such as TLRs 2, 3, 4, 7, and 9, the TLR adapter MyD88, as well as the inflammasome sensor NLRP3 and the inflammasome-dependent pro-inflammatory cytokines IL-1β and IL-18 (Fig. 7E). Because we observed that CD increased the endogenous LXR agonist 27-hydroxycholesterol, we next analyzed whether CD regulates the expression of LXR target genes in human atherosclerotic plaques. Indeed, GSEA revealed an enrichment of LXR target genes after CD treatment when compared to control treated plaques (Fig. 7F, Table S2). Additionally, many LXR target genes were found among the most differentially regulated genes (Fig. 7G, red or blue gene labels). Of note, the inflammasome sensor *NLRP3* and the inflammasome inhibitor *HSP90 (34)* are both LXR target genes *(24)*, and CD treatment resulted in *NLRP3* down-regulation and an up-regulation of *HSP90* when compared to control (Fig. 7H). Together these data show that CD activates LXR-dependent transcriptional programs in human plaques, influencing both cholesterol transport and several inflammatory processes, which are known to be relevant to the pathogenesis of atherosclerosis.

*Atheroprotection by cyclodextrin is LXR-dependent.*

We next tested whether the CD-mediated effects in isolated macrophages *in vitro* or in *ex vivo* treated human plaque material reflect the atheroprotective effects of CD in mice. Because CD treatment lowered the systemic concentrations of LXR-modulated cytokines (IL-1β, IL-6, and TNF-α) (Fig. 1H-J) and also resulted in increased *Abca1* and *Abcg1* mRNA in the aortic arches of $ApoE^{-/-}$ mice fed a cholesterol-rich diet (Fig. S7), we determined whether CD-mediated

atheroprotection *in vivo* requires LXR activation and cholesterol efflux from macrophages via ABCA1 and ABCG1. We therefore transplanted WT, LXR$\alpha^{-/-}\beta^{-/-}$, or macrophage specific ABCA1 and ABCG1 knockout (MAC-$ABC^{DKO}$) bone marrow into irradiated $LDLR^{-/-}$ mice. After bone marrow engraftment, the transplanted mice were fed a cholesterol-rich diet and were concomitantly treated with CD or vehicle control for eight weeks. CD treatment did not influence plasma cholesterol concentrations in the different transplant groups (Fig. 8A-C). The lipoprotein profiles also remained unchanged, except that CD treatment slightly decreased the amount of HDL in $LDLR^{-/-}$ mice transplanted with MAC-$ABC^{DKO}$ bone marrow (Fig. S8). $LDLR^{-/-}$ mice carrying WT bone marrow showed reduced atherosclerotic plaque size, demonstrating that CD is also effective in the $LDLR^{-/-}$ model of atherosclerosis (Fig. 8D). Of note, CD treatment did not influence lesion development in $LDLR^{-/-}$ mice carrying LXR$\alpha^{-/-}\beta^{-/-}$ bone marrow, highlighting the fact that LXR agonism is critical for CD-mediated atheroprotection (Fig. 8E). In contrast, deficiency of ABCA1 and ABCG1 in macrophages did not influence the effectiveness of CD treatment (Fig. 8F), suggesting that CD can bypass these cholesterol efflux pathways.

To better understand how CD-dependent LXR agonism can ameliorate atherosclerosis, we performed a genome-wide gene expression analysis on aortic tissue from $LDLR^{-/-}$ mice transplanted with WT or LXR$\alpha^{-/-}\beta^{-/-}$ bone marrow. GOEA of differentially expressed genes demonstrated that important pathways involved in atherogenesis, including lipid metabolism and inflammation, were regulated by CD treatment in an LXR-dependent manner (Fig. 8G). Similar to our studies on human plaques, LXR target genes were found among the top differentially regulated genes upon CD treatment (Fig. 8H). Moreover, we confirmed our observation from human plaques that CD promoted up-regulation of the NLRP3 inhibitor *Hsp90aa1* and down-regulation of NLRP3 inflammasome genes in an LXR-dependent manner (Fig. 8I). Together these data suggest that the CD-mediated atheroprotection observed in murine atherosclerosis is dependent on LXR activation and that CD exerts multiple anti-inflammatory effects in atherosclerotic plaques.

## Discussion

In this study, we tested the hypothesis that increasing the solubility of cholesterol by pharmacological means can have beneficial effects on diet-induced atherosclerosis. The large effect observed and the unexpected ability of CD to promote regression of established atherosclerosis even under the extreme hypercholesterolemic conditions observed during a cholesterol-rich diet cannot be explained by simple mass action of CD alone. The results from the lipid and genomic discovery approaches combined with *in vivo* studies in gene-deficient mice suggest that CD exerts its potent effect mainly by reprogramming cells in atherosclerotic plaques. By increasing the amount of endogenous LXR ligands, CD acts akin to a pro-drug except that it is not metabolized itself but rather promotes the metabolism of its cargo cholesterol into pharmacologically active metabolites.

It appears that transitory changes in cholesterol metabolism and inflammatory pathways are linked and that the activity of LXR is a key rheostat in this system. For example, innate immune activation by microbial components or the acute phase response can suppress expression of LXR target genes, such as *ABCA1* and *ABCG1*, causing cholesterol retention, which can augment an inflammatory reaction in various ways *(35, 36)*. Indeed, it is conceivable that this type of innate immune amplification could be part of an evolutionarily conserved antimicrobial defense mechanism *(23)*. The resulting cholesterol accumulation increases LXR agonists, which in turn

can counterbalance the inflammatory response and increase cholesterol efflux, restoring cholesterol and immune homeostasis. However, because of the overabundance of pro-inflammatory dietary factors and an excess of cholesterol, this balance may be shifted towards chronic inflammation and cholesterol retention, which drive atherogenesis. By promoting cholesterol solubility, enhancing LXR activity, and mobilizing cholesterol efflux, CD could therefore normalize both cholesterol and immune homeostasis in the vasculature.

The effect of CD on macrophages resembles that of the anti-atherogenic factor HDL. HDL relieves cells of excess cholesterol via ABC transporters and, in addition, HDL can have dramatic anti-inflammatory effects on macrophages *(37)*. However, HDL does not activate LXR but increases the expression of Activating Transcription Factor (ATF) 3, a key repressor of innate immune pathways *(37)*. In contrast, although CD has the ability to increase HDL-mediated RCT, it can also mobilize cholesterol for direct excretion into the urine and feces. These data suggest that CD can bypass ABCA1- and ABCG1-mediated active cholesterol efflux. Consistent with these observations, our bone marrow transplantation studies indicate that the atheroprotective effects of CD are independent of the active cholesterol efflux process mediated by ABCA1 and ABCG1. This is in line with recent findings demonstrating that synthetic LXR agonists mediate atheroprotection independent of macrophage ABCA1 and ABCG1 *(38)*.

There are several limitations to our study. First, although our data demonstrate that CD promotes LXR activation in plaque macrophages and that LXR is required in myeloid cells for CD-mediated atheroprotection, we cannot exclude other unidentified pathways. Indeed, it is likely that CD-mediated atheroprotection is multifactorial and that the differential effects of CD such as physically increasing cholesterol solubility, promoting cholesterol metabolism and efflux in macrophages, as well as its anti-inflammatory properties cannot easily be isolated. Second, although our data identified 27-hydroxycholesterol as the primary LXR agonist upon CD treatment, other endogenous oxysterols may also contribute to LXR activation. In this context, functional activity of regulatory enzymes such as Cyp27A1 and differential effects in specific cell types would be interesting. Third, although our *ex vivo* experiments with carotid artery plaques suggest that CD can induce atheroprotective pathways in human disease, specific clinical trials are necessary to validate these findings.

Preclinical models showing the effectiveness of LXR agonism in preventing murine atherosclerosis *(39)* and promoting atherosclerosis regression *(40)* provided promising prospects for clinical use of LXR agonists in atherosclerosis treatment, but the progression of therapeutic molecules into the clinic was hampered by liver toxicity and lipogenic effects *(41)*. CD, on the other hand, is already in clinical use in humans for the delivery of lipophilic drugs and has not shown relevant toxicity. Hence repurposing CD for the treatment or prevention of atherosclerosis would be feasible. Our studies provide a proof-of-principle that therapies aimed at increasing the solubility and removal of macrophage cholesterol could be an effective strategy for the treatment of atherosclerosis.

**Materials and methods:**

See supplementary files.

**Supplementary Materials:**

Materials and Methods

Fig. S1. CD treatment does not influence general cardiovascular parameters.

Fig. S2. CD treatment does not alter plasma sterol concentrations in atherosclerosis regression trials.

Fig. S3. 10 mM CD does not affect the viability of murine macrophages.

Fig. S4. CD mediates intracellular CC dissolution.

Fig. S5. CC loading of macrophages induces lipid droplet accumulation.

Fig. S6. CD does not affect Cyp27a1 expression.

Fig. S7. CD treatment induces the expression of cholesterol efflux transporters in the aortic arch of atherosclerotic mice.

Fig. S8. CD treatment does not alter murine lipoprotein profiles.

Table S1. LXR target gene list for GSEA analysis of BMDMs from WT and LXR$\alpha^{-/-}\beta^{-/-}$ mice.

Table S2. LXR target gene list for GSEA analysis of human atherosclerotic plaques.

Table S3. List of additional metabolic and regulatory genes (nCounter Panel Plus).

Table S4. Original data for all figures.

**References and notes:**

1. J. G. Robinson, M. Farnier, M. Krempf, J. Bergeron, G. Luc, M. Averna, E. S. Stroes, G. Langslet, F. J. Raal, M. E. Shahawy, M. J. Koren, N. E. Lepor, C. Lorenzato, R. Pordy, U. Chaudhari, J. J. P. Kastelein, ODYSSEY LONG TERM Investigators, Efficacy and Safety of Alirocumab in Reducing Lipids and Cardiovascular Events, *N Engl J Med* (2015), doi:10.1056/NEJMoa1501031.

2. M. S. Sabatine, R. P. Giugliano, S. D. Wiviott, F. J. Raal, D. J. Blom, J. Robinson, C. M. Ballantyne, R. Somaratne, J. Legg, S. M. Wasserman, R. Scott, M. J. Koren, E. A. Stein, Open-Label Study of Long-Term Evaluation against LDL Cholesterol (OSLER) Investigators, Efficacy and Safety of Evolocumab in Reducing Lipids and Cardiovascular Events, *N Engl J Med*, 150315080057008 (2015).

3. Task Force Members, G. Montalescot, U. Sechtem, S. Achenbach, F. Andreotti, C. Arden, A. Budaj, R. Bugiardini, F. Crea, T. Cuisset, C. Di Mario, J. R. Ferreira, B. J. Gersh, A. K. Gitt, J. S. Hulot, N. Marx, L. H. Opie, M. Pfisterer, E. Prescott, F. Ruschitzka, M. Sabate, R. Senior, D. P. Taggart, E. E. van der Wall, C. J. M. Vrints, ESC Committee for Practice Guidelines (CPG):, J. L. Zamorano, H. Baumgartner, J. J. Bax, H. Bueno, V. Dean, C. Deaton, C. Erol, R. Fagard, R. Ferrari, D. Hasdai, A. W. Hoes, P. Kirchhof, J. Knuuti, A. Linhart, P. Nihoyannopoulos, M. F. Piepoli, P. Ponikowski, P. A. Sirnes, J. L. Tamargo, M. Tendera, A. Torbicki, W. Wijns, S. Windecker, Document Reviewers:, M. Valgimigli, H. Bueno, M. J. Claeys, N. Donner-Banzhoff, C. Erol, H. Frank, C. Funck-Brentano, O. Gaemperli, J. R. Gonzalez-Juanatey, M. Hamilos, S. Husted, S. K. James, K. Kervinen, P. Kolh, S. D. Kristensen, P. Lancellotti, A. P. Maggioni, M.

F. Piepoli, A. R. Pries, F. Romeo, L. Ryden, M. L. Simoons, P. G. Steg, A. Timmis, A. Yildirir, 2013 ESC guidelines on the management of stable coronary artery disease: The Task Force on the management of stable coronary artery disease of the European Society of Cardiology, *Eur Heart J* **34**, 2949–3003 (2013).

4. F. J. Sheedy, A. Grebe, K. J. Rayner, P. Kalantari, B. Ramkhelawon, S. B. Carpenter, C. E. Becker, H. N. Ediriweera, A. E. Mullick, D. T. Golenbock, L. M. Stuart, E. Latz, K. A. Fitzgerald, K. J. Moore, CD36 coordinates NLRP3 inflammasome activation by facilitating intracellular nucleation of soluble ligands into particulate ligands in sterile inflammation, *Nat Immunol* **14**, 812–820 (2013).

5. P. Duewell, H. Kono, K. J. Rayner, C. M. Sirois, G. Vladimer, F. G. Bauernfeind, G. S. Abela, L. Franchi, G. Nuñez, M. Schnurr, T. Espevik, E. Lien, K. A. Fitzgerald, K. L. Rock, K. J. Moore, S. D. Wright, V. Hornung, E. Latz, NLRP3 inflammasomes are required for atherogenesis and activated by cholesterol crystals, *Nature* **464**, 1357–1361 (2010).

6. P. M. Ridker, T. Thuren, A. Zalewski, P. Libby, Interleukin-1β inhibition and the prevention of recurrent cardiovascular events: rationale and design of the Canakinumab Anti-inflammatory Thrombosis Outcomes Study (CANTOS), *Am. Heart J.* **162**, 597–605 (2011).

7. A. Warnatsch, M. Ioannou, Q. Wang, V. Papayannopoulos, Inflammation. Neutrophil extracellular traps license macrophages for cytokine production in atherosclerosis, *Science* **349**, 316–320 (2015).

8. S. Nymo, N. Niyonzima, T. Espevik, T. E. Mollnes, Cholesterol crystal-induced endothelial cell activation is complement-dependent and mediated by TNF, *Immunobiology* **219**, 786–792 (2014).

9. E. O. Samstad, N. Niyonzima, S. Nymo, M. H. Aune, L. Ryan, S. S. Bakke, K. T. Lappegård, O.-L. Brekke, J. D. Lambris, J. K. Damås, E. Latz, T. E. Mollnes, T. Espevik, Cholesterol crystals induce complement-dependent inflammasome activation and cytokine release, *J Immunol* **192**, 2837–2845 (2014).

10. R. Kiyotake, M. Oh-Hora, E. Ishikawa, T. Miyamoto, T. Ishibashi, S. Yamasaki, Human Mincle Binds to Cholesterol Crystals and Triggers Innate Immune Responses, *J Biol Chem*, jbc.M115.645234 (2015).

11. K. J. Rayner, C. C. Esau, F. N. Hussain, A. L. McDaniel, S. M. Marshall, J. M. van Gils, T. D. Ray, F. J. Sheedy, L. Goedeke, X. Liu, O. G. Khatsenko, V. Kaimal, C. J. Lees, C. Fernández-Hernando, E. A. Fisher, R. E. Temel, K. J. Moore, Inhibition of miR-33a/b in non-human primates raises plasma HDL and lowers VLDL triglycerides, *Nature* **478**, 404–407 (2011).

12. S. Gould, R. C. Scott, 2-Hydroxypropyl-beta-cyclodextrin (HP-beta-CD): a toxicology review, *Food Chem. Toxicol.* **43**, 1451–1459 (2005).

13. T. Loftsson, P. Jarho, M. Másson, T. Järvinen, Cyclodextrins in drug delivery, *Expert Opin Drug Deliv* **2**, 335–351 (2005).

14. S. M. Liu, A. Cogny, M. Kockx, R. T. Dean, K. Gaus, W. Jessup, L. Kritharides,

Cyclodextrins differentially mobilize free and esterified cholesterol from primary human foam cell macrophages, *J Lipid Res* **44**, 1156–1166 (2003).

15. L. Kritharides, M. Kus, A. J. Brown, W. Jessup, R. T. Dean, Hydroxypropyl-beta-cyclodextrin-mediated efflux of 7-ketocholesterol from macrophage foam cells, *J Biol Chem* **271**, 27450–27455 (1996).

16. V. M. Atger, M. de la Llera Moya, G. W. Stoudt, W. V. Rodrigueza, M. C. Phillips, G. H. Rothblat, Cyclodextrins as catalysts for the removal of cholesterol from macrophage foam cells, *J. Clin. Invest.* **99**, 773–780 (1997).

17. D. S. Mackay, P. J. H. Jones, Plasma noncholesterol sterols: current uses, potential and need for standardization, *Curr. Opin. Lipidol.* **23**, 241–247 (2012).

18. G. S. Getz, C. A. Reardon, Animal models of atherosclerosis, *Arterioscler Thromb Vasc Biol* **32**, 1104–1115 (2012).

19. B. Hewing, E. A. Fisher, Preclinical mouse models and methods for the discovery of the causes and treatments of atherosclerosis, *Expert Opin Drug Discov* **7**, 207–216 (2012).

20. K. J. Rayner, F. J. Sheedy, C. C. Esau, F. N. Hussain, R. E. Temel, S. Parathath, J. M. van Gils, A. J. Rayner, A. N. Chang, Y. Suárez, C. Fernández-Hernando, E. A. Fisher, K. J. Moore, Antagonism of miR-33 in mice promotes reverse cholesterol transport and regression of atherosclerosis, *J. Clin. Invest.* **121**, 2921–2931 (2011).

21. I. Tabas, Consequences of cellular cholesterol accumulation: basic concepts and physiological implications, *J. Clin. Invest.* **110**, 905–911 (2002).

22. J. J. Repa, D. J. Mangelsdorf, The liver X receptor gene team: potential new players in atherosclerosis, *Nat Med* **8**, 1243–1248 (2002).

23. A. R. Tall, L. Yvan-Charvet, Cholesterol, inflammation and innate immunity, *Nature Reviews Immunology* **15**, 104–116 (2015).

24. A. Reboldi, E. V. Dang, J. G. McDonald, G. Liang, D. W. Russell, J. G. Cyster, Inflammation. 25-Hydroxycholesterol suppresses interleukin-1-driven inflammation downstream of type I interferon, *Science* **345**, 679–684 (2014).

25. A. V. Khera, M. Cuchel, M. de la Llera-Moya, A. Rodrigues, M. F. Burke, K. Jafri, B. C. French, J. A. Phillips, M. L. Mucksavage, R. L. Wilensky, E. R. Mohler, G. H. Rothblat, D. J. Rader, Cholesterol efflux capacity, high-density lipoprotein function, and atherosclerosis, *N Engl J Med* **364**, 127–135 (2011).

26. A. Rohatgi, A. Khera, J. D. Berry, E. G. Givens, C. R. Ayers, K. E. Wedin, I. J. Neeland, I. S. Yuhanna, D. R. Rader, J. A. de Lemos, P. W. Shaul, HDL cholesterol efflux capacity and incident cardiovascular events, *N Engl J Med* **371**, 2383–2393 (2014).

27. D. J. Rader, E. Puré, Lipoproteins, macrophage function, and atherosclerosis: beyond the foam cell? *Cell Metab.* **1**, 223–230 (2005).

28. B. A. Janowski, P. J. Willy, T. R. Devi, J. R. Falck, D. J. Mangelsdorf, An oxysterol signalling pathway mediated by the nuclear receptor LXR alpha, *Nature* **383**, 728–731 (1996).

29. A. Subramanian, P. Tamayo, V. K. Mootha, S. Mukherjee, B. L. Ebert, M. A. Gillette, A. Paulovich, S. L. Pomeroy, T. R. Golub, E. S. Lander, J. P. Mesirov, Gene set enrichment analysis: a knowledge-based approach for interpreting genome-wide expression profiles, *Proc Natl Acad Sci USA* **102**, 15545–15550 (2005).

30. S. Heinz, C. Benner, N. Spann, E. Bertolino, Y. C. Lin, P. Laslo, J. X. Cheng, C. Murre, H. Singh, C. K. Glass, Simple combinations of lineage-determining transcription factors prime cis-regulatory elements required for macrophage and B cell identities, *Mol. Cell* **38**, 576–589 (2010).

31. J. J. Repa, S. D. Turley, J. A. Lobaccaro, J. Medina, L. Li, K. Lustig, B. Shan, R. A. Heyman, J. M. Dietschy, D. J. Mangelsdorf, Regulation of absorption and ABC1-mediated efflux of cholesterol by RXR heterodimers, *Science* **289**, 1524–1529 (2000).

32. B. Liu, H. Li, J. J. Repa, S. D. Turley, J. M. Dietschy, Genetic variations and treatments that affect the lifespan of the NPC1 mouse, *J Lipid Res* **49**, 663–669 (2008).

33. A. M. Taylor, B. Liu, Y. Mari, B. Liu, J. J. Repa, Cyclodextrin mediates rapid changes in lipid balance in Npc1-/- mice without carrying cholesterol through the bloodstream, *J Lipid Res* **53**, 2331–2342 (2012).

34. A. Mayor, F. Martinon, T. De Smedt, V. Pétrilli, J. Tschopp, A crucial function of SGT1 and HSP90 in inflammasome activity links mammalian and plant innate immune responses, *Nat Immunol* **8**, 497–503 (2007).

35. A. Castrillo, S. B. Joseph, S. A. Vaidya, M. Haberland, A. M. Fogelman, G. Cheng, P. Tontonoz, Crosstalk between LXR and toll-like receptor signaling mediates bacterial and viral antagonism of cholesterol metabolism, *Mol. Cell* **12**, 805–816 (2003).

36. K. R. Feingold, C. Grunfeld, The acute phase response inhibits reverse cholesterol transport, *J Lipid Res* **51**, 682–684 (2010).

37. D. De Nardo, L. I. Labzin, H. Kono, R. Seki, S. V. Schmidt, M. Beyer, D. Xu, S. Zimmer, C. Lahrmann, F. A. Schildberg, J. Vogelhuber, M. Kraut, T. Ulas, A. Kerksiek, W. Krebs, N. Bode, A. Grebe, M. L. Fitzgerald, N. J. Hernandez, B. R. G. Williams, P. Knolle, M. Kneilling, M. Röcken, D. Lütjohann, S. D. Wright, J. L. Schultze, E. Latz, High-density lipoprotein mediates anti-inflammatory reprogramming of macrophages via the transcriptional regulator ATF3, *Nat Immunol* **15**, 152–160 (2014).

38. M. S. Kappus, A. J. Murphy, S. Abramowicz, V. Ntonga, C. L. Welch, A. R. Tall, M. Westerterp, Activation of liver X receptor decreases atherosclerosis in Ldlr$^{-/-}$ mice in the absence of ATP-binding cassette transporters A1 and G1 in myeloid cells, *Arterioscler Thromb Vasc Biol* **34**, 279–284 (2014).

39. S. B. Joseph, E. McKilligin, L. Pei, M. A. Watson, A. R. Collins, B. A. Laffitte, M. Chen, G. Noh, J. Goodman, G. N. Hagger, J. Tran, T. K. Tippin, X. Wang, A. J. Lusis, W. A. Hsueh, R. E. Law, J. L. Collins, T. M. Willson, P. Tontonoz, Synthetic LXR ligand inhibits the development

of atherosclerosis in mice, *Proc Natl Acad Sci USA* **99**, 7604–7609 (2002).

40. J. E. Feig, I. Pineda-Torra, M. Sanson, M. N. Bradley, Y. Vengrenyuk, D. Bogunovic, E. L. Gautier, D. Rubinstein, C. Hong, J. Liu, C. Wu, N. van Rooijen, N. Bhardwaj, M. Garabedian, P. Tontonoz, E. A. Fisher, LXR promotes the maximal egress of monocyte-derived cells from mouse aortic plaques during atherosclerosis regression, *J. Clin. Invest.* **120**, 4415–4424 (2010).

41. X. Li, V. Yeh, V. Molteni, Liver X receptor modulators: a review of recently patented compounds (2007 - 2009), *Expert Opin Ther Pat* **20**, 535–562 (2010).

42. V. Hornung, F. Bauernfeind, A. Halle, E. O. Samstad, H. Kono, K. L. Rock, K. A. Fitzgerald, E. Latz, Silica crystals and aluminum salts activate the NALP3 inflammasome through phagosomal destabilization, *Nat Immunol* **9**, 847–856 (2008).

43. S. Wassmann, A. T. Bäumer, K. Strehlow, M. van Eickels, C. Grohé, K. Ahlbory, R. Rösen, M. Böhm, G. Nickenig, Endothelial dysfunction and oxidative stress during estrogen deficiency in spontaneously hypertensive rats, *Circulation* **103**, 435–441 (2001).

44. D. Lütjohann, C. Hahn, W. Prange, T. Sudhop, M. Axelson, T. Sauerbruch, K. von Bergmann, C. Reichel, Influence of rifampin on serum markers of cholesterol and bile acid synthesis in men, *Int J Clin Pharmacol Ther* **42**, 307–313 (2004).

45. D. Lütjohann, A. Brzezinka, E. Barth, D. Abramowski, M. Staufenbiel, K. von Bergmann, K. Beyreuther, G. Multhaup, T. A. Bayer, Profile of cholesterol-related sterols in aged amyloid precursor protein transgenic mouse brain, *J Lipid Res* **43**, 1078–1085 (2002).

46. S. Zimmer, M. Steinmetz, T. Asdonk, I. Motz, C. Coch, E. Hartmann, W. Barchet, S. Wassmann, G. Hartmann, G. Nickenig, Activation of endothelial toll-like receptor 3 impairs endothelial function, *Circ Res* **108**, 1358–1366 (2011).

47. J. Spandl, D. J. White, J. Peychl, C. Thiele, Live Cell Multicolor Imaging of Lipid Droplets with a New Dye, LD540, *Traffic* **10**, 1579–1584 (2009).

48. D. Lütjohann, M. Stroick, T. Bertsch, S. Kühl, B. Lindenthal, K. Thelen, U. Andersson, I. Björkhem, K. V. Bergmann Kv, K. Fassbender, High doses of simvastatin, pravastatin, and cholesterol reduce brain cholesterol synthesis in guinea pigs, *Steroids* **69**, 431–438 (2004).

49. D. Lütjohann, O. Breuer, G. Ahlborg, I. Nennesmo, A. Sidén, U. Diczfalusy, I. Björkhem, Cholesterol homeostasis in human brain: evidence for an age-dependent flux of 24S-hydroxycholesterol from the brain into the circulation, *Proc Natl Acad Sci USA* **93**, 9799–9804 (1996).

50. S. Maere, K. Heymans, M. Kuiper, BiNGO: a Cytoscape plugin to assess overrepresentation of gene ontology categories in biological networks, *Bioinformatics* **21**, 3448–3449 (2005).

51. D. Merico, R. Isserlin, O. Stueker, A. Emili, G. D. Bader, T. Ravasi, Ed. Enrichment map: a network-based method for gene-set enrichment visualization and interpretation, *PLoS ONE* **5**, e13984 (2010).

52. L. Oesper, D. Merico, R. Isserlin, G. D. Bader, WordCloud: a Cytoscape plugin to create a visual semantic summary of networks, *Source Code Biol Med* **6**, 7 (2011).

53. T. G. Brott, J. L. Halperin, S. Abbara, J. M. Bacharach, J. D. Barr, R. L. Bush, C. U. Cates, M. A. Creager, S. B. Fowler, G. Friday, V. S. Hertzberg, E. B. McIff, W. S. Moore, P. D. Panagos, T. S. Riles, R. H. Rosenwasser, A. J. Taylor, American College of Cardiology, American Stroke Association, American Association of Neurological Surgeons, American College of Radiology, American American College of Radiology, Society of NeuroInterventional Surgery, Society for Vascular Medicine, Society for Vascular Surgery, 2011 ASA/ACCF/AHA/AANN/AANS/ACR/ASNR/CNS/SAIP/SCAI/SIR/SNIS/SVM/SVS guideline on the management of patients with extracranial carotid and vertebral artery disease. A report of the American College of Cardiology Foundation/American Heart Association Task Force on Practice Guidelines, and the American Stroke Association, American Association of Neuroscience Nurses, American Association of Neurological Surgeons, American College of Radiology, American Society of Neuroradiology, Congress of Neurological Surgeons, Society of Atherosclerosis Imaging and Prevention, Society for Cardiovascular Angiography and Interventions, Society of Interventional Radiology, Society of NeuroInterventional Surgery, Society for Vascular Medicine, and Society for Vascular Surgery.*Circulation* **124**, e54–130 (2011).

54. D. S. Mackay, P. J. H. Jones, S. B. Myrie, J. Plat, D. Lütjohann, Methodological considerations for the harmonization of non-cholesterol sterol bio-analysis, *J. Chromatogr. B Analyt. Technol. Biomed. Life Sci.* **957**, 116–122 (2014).

55. P. Pehkonen, L. Welter-Stahl, J. Diwo, J. Ryynänen, A. Wienecke-Baldacchino, S. Heikkinen, E. Treuter, K. R. Steffensen, C. Carlberg, Genome-wide landscape of liver X receptor chromatin binding and gene regulation in human macrophages, *BMC Genomics* **13**, 50 (2012).

56. E. B. Mathiesen, K. H. Bønaa, O. Joakimsen, Echolucent plaques are associated with high risk of ischemic cerebrovascular events in carotid stenosis: the tromsø study, *Circulation* **103**, 2171–2175 (2001).

57. P. S. Olofsson, K. Jatta, D. Wågsäter, S. Gredmark, U. Hedin, G. Paulsson-Berne, C. Söderberg-Nauclér, G. K. Hansson, A. Sirsjö, The antiviral cytomegalovirus inducible gene 5/viperin is expressed in atherosclerosis and regulated by proinflammatory agents, *Arterioscler Thromb Vasc Biol* **25**, e113–6 (2005).

**Acknowledgments:** We appreciate the great technical assistance of Catharina Lahrmann, Anna Glubokovskih, Gudrun Hack und Silke Bellinghausen (University of Bonn, Bonn, Germany), Anne Marstad (Norwegian University of Science and Technology, Trondheim, Norway), Zeina Ali (Karolinska Institute, Huddinge, Sweden) and Kirsten Krohg Sørensen (Oslo University Hospital, Oslo, Norway). We thank Caroline Hastings (Children's Hospital & Research Center Oakland, Oakland, CA, USA) for help with the acquisition of samples from NPC patients and greatly appreciate the contribution of the Hadley Hope Fund (Medford, OR, USA). 2-hydroxypropyl-β-cyclodextrin as well as 2-hydroxypropyl-β-cyclodextrin-rhodamine was kindly provided by CTD Holdings, Inc., Alachua, FL, USA. LD540 was generously provided by Christoph Thiele (University of Bonn, Bonn, Germany).

**Funding**: This work was funded by grants of the National Institutes of Health R01-HL093262, R21-HL113907-01 (to E.L.), HL112661-01 (to M.L.F. and E.L.), HL101274 (to M.L.F.), HL107653 (to A.R.T.), by the Research Council of Norway through its Centres of Excellence funding scheme, project number 223255/F50 (to S.S.B, E.L. and T.E.), by BONFOR (to S.Z. and N.B.), by the Robert A. Welch Foundation (E-0004, to J.A.G), by the Swedish Science Council (H2416223, to J.A.G.) and by grants of the Deutsche Forschungsgemeinschaft (DFG SFB645, SFB670, SFB704, TRR83, TRR57) (to E.L., J.L.S. and J.T.). E.L, M.T.H. and J.L.S. are members of the Excellence cluster ImmunoSensation (Exc1023) funded by the DFG.

**Author contributions**: S.Z., A.G. designed, performed and analyzed experiments. N.B. assisted with atherosclerosis mouse models and data analysis. S.S.B., L.I.L., B.H., M.S., J.T., A.K. and V.H. performed experiments. S.S.B., T.U. and J.L.S. performed bioinformatic analyses. J.A.G., M.T.H., I.B., M.W. and A.R.T. provided knock-out mice. D.D., G.N., T.E., M.L.F., S.D.W., and D.L. analyzed data and provided critical suggestions and discussions throughout the study. C.H. provided the initial idea for the study. S.Z., A.G. and E.L. designed the study and wrote the manuscript.

**Competing interests**: S.D.W. is a full-time employee of CSL Limited, which does not work with cyclodextrin. All authors declare that they have no competing interests.

**Data and materials availability**: Accession codes for data in Gene Expression Omnibus (GEO): GSE67014 includes GSE67011 and GSE67013.

**Figures**:

**Fig. 1. CD treatment impairs murine atherogenesis.** ApoE$^{-/-}$ mice were fed a cholesterol-rich diet for eight weeks and concomitantly treated with 2 g CD/ kg body weight or vehicle control by subcutaneous injection twice a week (n=7-8 per group). **(A)** Plasma cholesterol concentrations. **(B)** Atherosclerotic plaque area relative to total arterial wall area. **(C)** Plaque CC load shown as ratio of crystal reflection area to plaque area. **(D)** Representative images of the aortic plaques obtained by confocal laser reflection microscopy. Macrophages stained with anti-CD68 antibodies (red), reflection signal of CCs (white), nuclei stained with Hoechst (blue). Enlarged areas are shown by white boxes. Scale bars indicate 500 μm. **(E)** Plaque cellularity shown as ratio of nuclei to plaque area. **(F)** Plaque macrophage load shown as ratio of CD68 fluorescence area to total plaque area. **(G)** Aortic superoxide production determined by L-012 chemiluminescence. Plasma **(H)** IL-1β, **(I)** TNF-α, and **(J)** IL-6 concentrations. Data are shown as mean + s.e.m. Control vs. CD, unpaired two-tailed Student's t test; ***$p < 0.001$, **$p < 0.01$, *$p < 0.05$, ns = not significant.

**Fig. 2. CD treatment facilitates regression of murine atherosclerosis.** ApoE$^{-/-}$ mice were fed a cholesterol-rich diet for eight weeks to induce advanced atherosclerotic lesions. Then the diet was either changed to a normal chow **(A-D)** or the cholesterol-rich diet was continued **(E-H)** for another four weeks. Mice were simultaneously treated with 2 g CD/ kg body weight or vehicle control twice a week (n=6-8 per group). **(A, E)** Diet and treatment schemes. **(B, F)** Plasma cholesterol concentrations. **(C, G)** Atherosclerotic plaque area relative to total arterial wall area.

**(D, H)** Plaque CC load shown as ratio of crystal reflection area to plaque area. Data are shown as mean + s.e.m., Control vs. CD, unpaired two-tailed Student's t test; ***p < 0.001, **p < 0.01, *p < 0.05, ns = not significant.

**Fig. 3. CD interacts with and dissolves extra- and intracellular CCs. (A, B)** 1 mg CCs were incubated in 0.5 mM rhodamine-labeled CD or PBS as control. **(A)** Representative images obtained by confocal laser reflection microscopy. Scale bar equals 20 µm. **(B)** Quantification of rhodamine fluorescence on CCs by flow cytometry. **(C)** $^{3}$H-CC were incubated in CD solutions of the indicated concentrations overnight, shaking at 37°C. Upon filtration through 0.22 µm filter plates, radioactivity was determined in the filtrate (filterable/solubilized) and the retentate (crystalline). **(D, E)** iMacs were loaded with 200 µg CC/1x10$^{6}$ cells for 3 hours before incubation with 1 mM rhodamine-labeled CD. **(D)** Quantification of rhodamine fluorescence by flow cytometry. **(E)** Representative images obtained by confocal microscopy; rhodamine-labeled CD (red), laser reflection signal (green). Scale bars equal 5 µm. **(F)** Intracellular CC dissolution in BMDMs treated with 10 mM CD or control for the indicated times determined by polarization microscopy. Data are shown as mean +/- s.e.m of at least three independent experiments.

**Fig. 4. CD mediates metabolism and efflux of crystal-derived cholesterol. (A)** Macrophages loaded with CCs prepared from $D_6$-cholesterol ($D_6$-CC) can reduce the amount of free, crystal-derived $D_6$-cholesterol by three main mechanisms. First, acetyl-CoA acetyltransferase (ACAT1) can catalyze the formation of $D_6$-cholesteryl esters, the storage form of cholesterol, which is deposited in lipid droplets. Second, the mitochondrial enzyme 27-hydroxylase (Cyp27A1) can catalyze the formation of $D_5$-27-hydroxycholesterol, which can passively diffuse across cell membranes. Third, $D_5$-27-hydroxycholesterol is a potent activator of LXR transcription factors, which in turn mediate the up-regulation of the cholesterol efflux transporters ABCA1 and ABCG1. **(B, C)** iMacs loaded with 200 µg $D_6$-CC/1x10$^{6}$ cells for 3 hours were treated with 10 mM CD or vehicle control before GC-MS-SIM analysis of crystal-derived cholesterol. **(B)** Percentage of esterified $D_6$-cholesterol in cell and supernatant fractions before CD treatment (control bar) and after 48 hours of CD treatment. **(C)** Efflux of $D_6$-cholesterol into supernatants of $D_6$-CC-loaded macrophages before CD treatment (control bar) and upon 24 hours of CD treatment. Gene expression of **(D)** *Abca1* and **(E)** *Abcg1*, and **(F)** protein expression of ABCA1 in BMDMs loaded with 100 µg CC/1x10$^{6}$ cells for 3 hours and then incubated with 10 mM CD or medium control for **(D, E)** 4 hours or **(F)** 24 hours. Immunoblot in **(F)** is representative of three independent experiments, and densitometric analysis of all three experiments is provided for 10 mM CD and presented as ABCA1 expression relative to the loading control β-ACTIN. Data are shown as means + s.e.m. of at least three independent experiments. **(G)** $D_5$-27-hydroxycholesterol in cell and supernatant fractions of iMacs loaded with 200 µg $D_6$-CC/1x10$^{6}$ cells for 3 hours before 48 hours of treatment with 10 mM CD or medium control, determined by GC-MS-SIM. **(H)** 27-hydroxycholesterol in cell and supernatant fractions of iMacs after 48 hours of treatment with 10 mM CD or medium control. **(B, C)** Medium vs. CD, unpaired two-tailed Student's t test; **(D-F)** CC+Control vs. CC+CD, unpaired two-tailed Student's t test; **(G, H)** Control vs. CD, unpaired two-tailed Student's t test; ***p < 0.001, *p < 0.05, ns = not significant.

**Fig. 5. CD induces LXR target gene expression in WT macrophages. (A)** BMDMs from WT and LXRα$^{-/-}$β$^{-/-}$ mice were loaded with 100 µg CC/1x10$^{6}$ cells for 3 hours and incubated with 10

mM CD for 4 hours for microarray analysis. GSEA for LXR target gene sets described in Heinz *et al. (30)* (Table S1) was performed on gene expression data. DB = data base. **(B, C)** GSEA results for **(B)** WT and **(C)** LXR$\alpha^{-/-}\beta^{-/-}$ BMDMs presented as volcano plots of normalized enrichment score (NES) and enrichment p-values. Red circles show positively and significantly enriched gene sets (NES>1, p-value<0.05). **(D-F)** Gene expression of **(D)** *Abca1* and **(E)** *Abcg1*, and **(F)** protein expression of ABCA1 in BMDMs from WT and LXR$\alpha^{-/-}\beta^{-/-}$ mice loaded with 100 μg CC/1x$10^6$ cells for 3 hours and then incubated with 10 mM CD for **(D, E)** 4 hours or **(F)** 24 hours. The synthetic LXR agonist T0901317 (10 μM) was used as a positive control for ABCA1 protein induction. Immunoblot in **(F)** is representative of two independent experiments. Data are shown as mean + s.e.m. of two independent experiments. CC+Control vs. CC+CD, unpaired two-tailed Student's t test; *p < 0.05.

**Fig. 6. CD facilitates RCT *in vivo* and promotes urinary cholesterol excretion. (A)** BMDMs from WT or LXR$\alpha^{-/-}\beta^{-/-}$ mice were loaded with 100 μg $D_6$-CC/1x$10^6$ cells and injected into the peritoneum of WT mice. Subsequently, mice were treated subcutaneously with 2 g CD/ kg body weight or vehicle control (n=4 per group). $D_6$-cholesterol content in **(B)** feces and **(C)** urine collected every 3 hours over 30 hours after CD injection. Data are shown as total area under the curve of excreted $D_6$-cholesterol pooled from the mice within a group per time point. **(D)** Urine samples collected from three individual NPC1 patients upon intravenous application of CD for specific treatment of NPC. Urine cholesterol concentration was determined by GC-MS-SIM and normalized to urine creatinine excretion.

**Fig. 7. CD induces cholesterol metabolism and an anti-inflammatory LXR profile in human atherosclerotic carotid plaques. (A)** Human atherosclerotic carotid plaques obtained by carotid endarterectomy (n=10) were split into two macroscopically equal pieces and cultured for 24 hours with 10 mM CD or control. Half of the plaque tissue was used for mRNA profiling with nCounter analysis system (Nanostring Technologies), and the other half and the culture supernatant were analyzed by GC-MS-SIM. **(B)** Cholesterol efflux from plaque tissue into supernatants displayed as % of total cholesterol per sample. **(C)** Distribution of 27-hydroxycholesterol relative to cholesterol in plaque and supernatant. **(D)** GOEA of differentially expressed (DE) genes (FC>1.3, p-value<0.05) visualized as GO network, where red nodes indicate GO term enrichment by up-regulated DE genes and blue borders indicate GO term enrichment by down-regulated DE genes. Node size and border width represent the corresponding FDR-adjusted enrichment p value (q value). Edges represent the associations between two enriched GO terms based on shared genes, and edge thickness indicates the overlap of genes between neighbor nodes. Highly connected terms were grouped together and were annotated manually by a shared general term. **(E)** Heat map of genes involved in the GO term "Regulation of inflammatory response" (GO:0050727). Color bar indicates fold change. **(F)** Volcano plot of NES and enrichment p-values based on GSEA for the LXR target gene set (Table S2). Red circle indicates positive and significant enrichment of the LXR target gene set (NES>1, p-value<0.05). **(G)** Top DE genes determined by 3-way ANOVA (FC>1.5, p-value<0.05). LXR target genes are colored in red or blue. **(H)** The expression of genes relevant to the NLRP3 inflammasome pathway. Color bar indicates fold change. **(B, C)** Data are shown as mean +/- s.e.m. CD vs. Control, paired two-tailed Student's t test; ***p < 0.001, *p < 0.05.

**Fig. 8. CD impairs atherogenesis and regulates metabolic and anti-inflammatory processes in an LXR-dependent manner.** $LDLR^{-/-}$ mice were transplanted with WT, $LXR\alpha^{-/-}\beta^{-/-}$, or $MAC\text{-}ABC^{DKO}$ bone marrow. They were then fed a cholesterol-rich diet for eight weeks and concomitantly treated with 2 g CD/ kg body weight or vehicle control twice a week (n=6-8 per group). **(A-C)** Plasma cholesterol concentrations of CD- and vehicle-treated animals. **(D-F)** Atherosclerotic plaque area relative to total arterial wall area. **(G-I)** Descending aortas of $LDLR^{-/-}$ mice transplanted with WT and $LXR\alpha^{-/-}\beta^{-/-}$ bone marrow were used for gene expression analysis by microarray, with subsequent filtration for the genes included in the human plaque mRNA profiling. **(G)** GOEA of differentially expressed (DE) genes (FC>1.3, p-value<0.05) visualized as GO network, where red nodes indicate GO term enrichment by up-regulated DE genes and blue borders indicate GO term enrichment by down-regulated DE genes. Node size and border width represent the corresponding FDR-adjusted enrichment p value (q value). Edges represent the associations between two enriched GO terms based on shared genes, and edge thickness indicates the overlap of genes between neighbor nodes. Highly connected terms were grouped together and were annotated manually by a shared general term. **(H)** DE genes determined by 3-way ANOVA (FC>1.3, p-value<0.05) in aortas of $LDLR^{-/-}$ mice transplanted with WT bone marrow. LXR target genes are colored in red or blue. **(I)** The expression of genes relevant for the NLRP3 inflammasome pathway. Color bar indicates fold change. **(A, B)** Data are shown as mean + s.e.m., CD vs. Control, unpaired two-tailed Student's t test; $^{**}p < 0.01$, $^{*}p < 0.05$.

## Figure 1

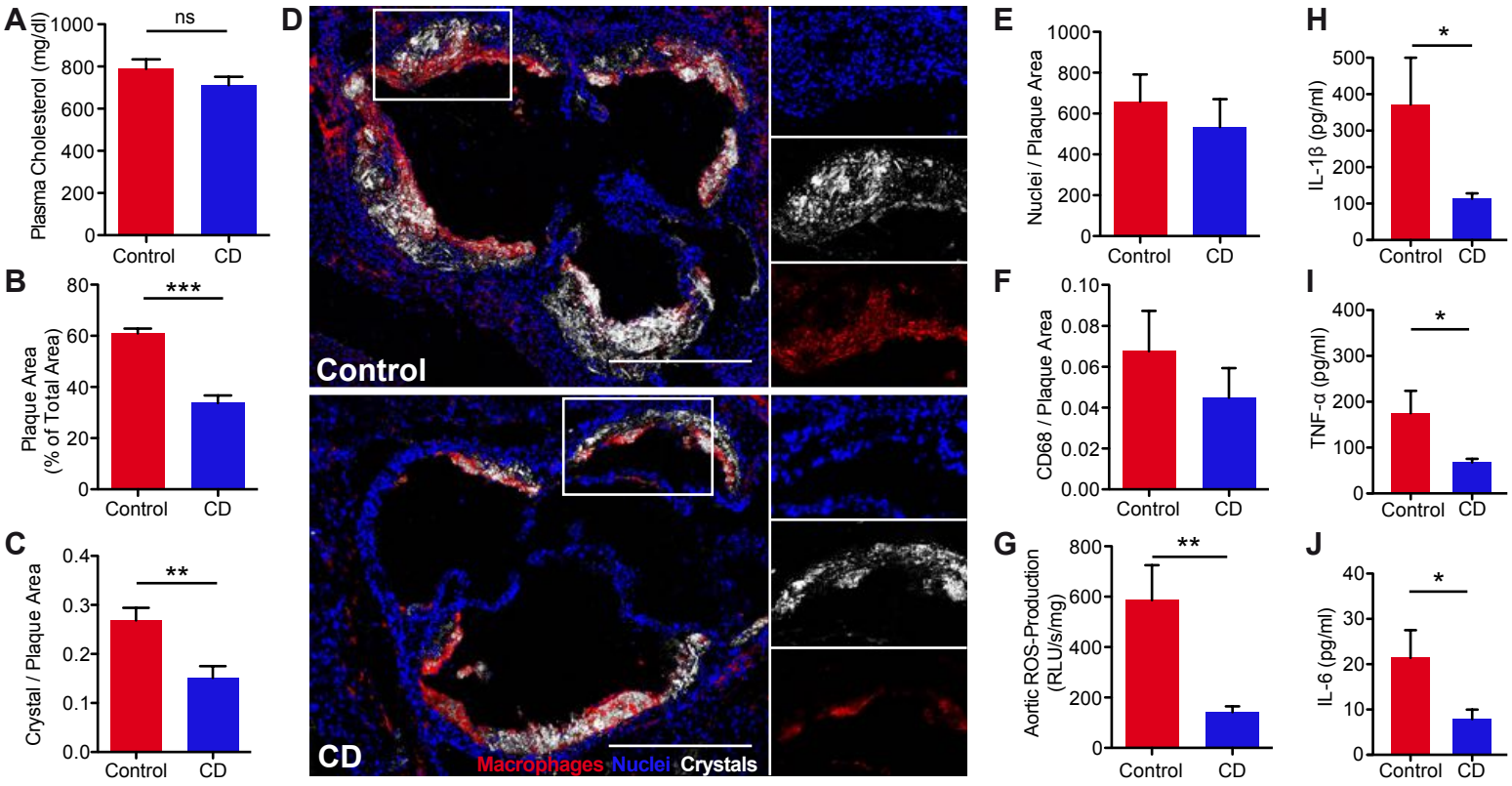
A
Plasma Cholesterol (mg/dl)
1000
800
600
400
200
0
ns
Control
CD
B
Plaque Area
(% of Total Area)
80
60
40
20
0
***
Control
CD
C
Crystal / Plaque Area
0.4
0.3
0.2
0.1
0.0
**
Control
CD
D
Control
CD
Macrophages
Nuclei
Crystals
E
Nuclei / Plaque Area
1000
800
600
400
200
0
Control
CD
F
CD68 / Plaque Area
0.10
0.08
0.06
0.04
0.02
0.00
Control
CD
G
Aortic ROS-Production
(RLU/s/mg)
800
600
400
200
0
**
Control
CD
H
IL-1β (pg/ml)
500
400
300
200
100
0
*
Control
CD
I
TNF-α (pg/ml)
400
300
200
100
0
*
Control
CD
J
IL-6 (pg/ml)
40
30
20
10
0
*
Control
CD

# Figure 2

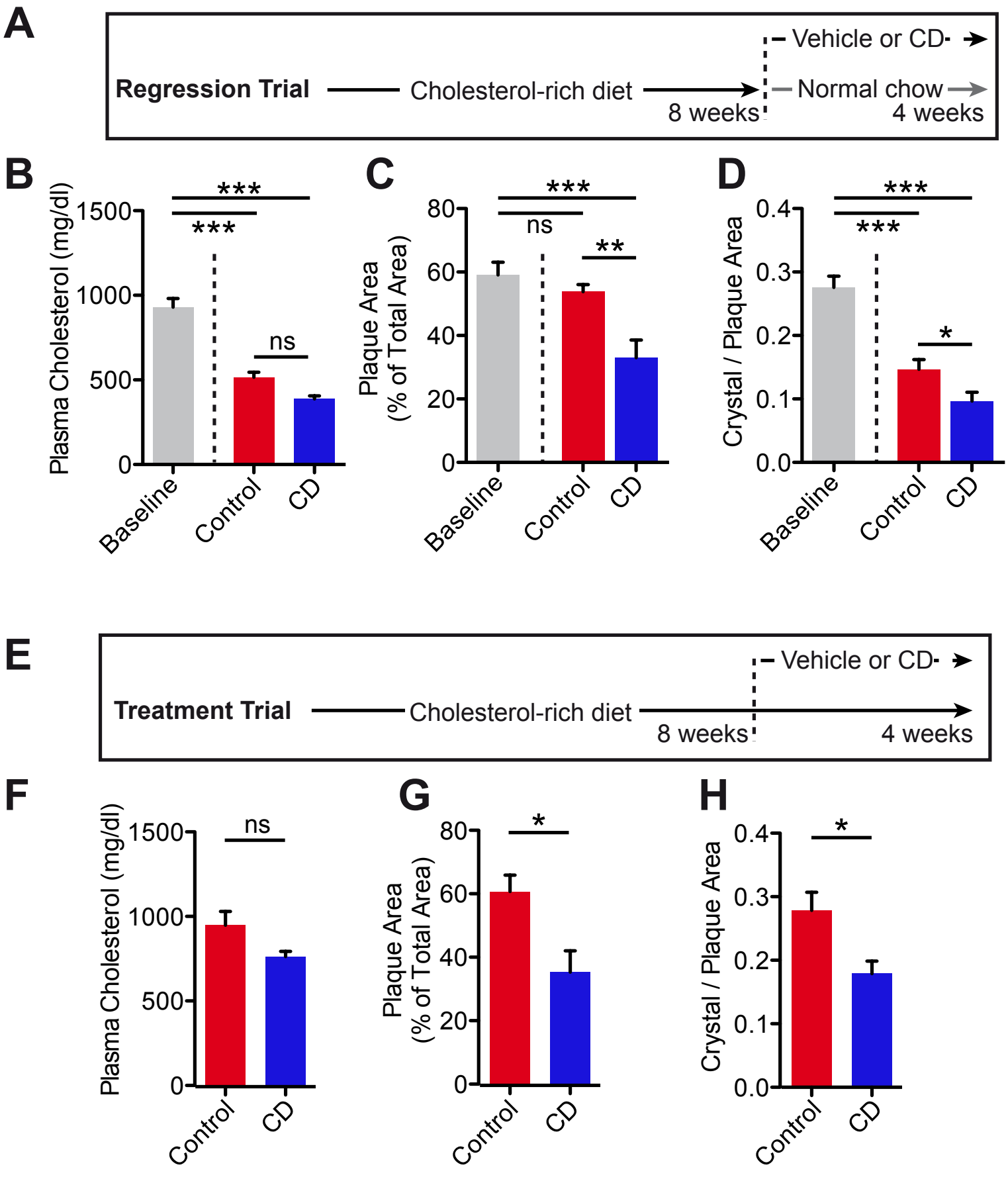
A
Regression Trial
Cholesterol-rich diet
8 weeks
Vehicle or CD
Normal chow
4 weeks
B
Plasma Cholesterol (mg/dl)
1500
1000
500
0
***
***
ns
Baseline
Control
CD
C
Plaque Area (% of Total Area)
80
60
40
20
0
***
ns
**
Baseline
Control
CD
D
Crystal / Plaque Area
0.4
0.3
0.2
0.1
0.0
***
***
*
Baseline
Control
CD
E
Treatment Trial
Cholesterol-rich diet
8 weeks
Vehicle or CD
4 weeks
F
Plasma Cholesterol (mg/dl)
1500
1000
500
0
ns
Control
CD
G
Plaque Area (% of Total Area)
80
60
40
20
0
*
Control
CD
H
Crystal / Plaque Area
0.4
0.3
0.2
0.1
0.0
*
Control
CD

**Figure 3**

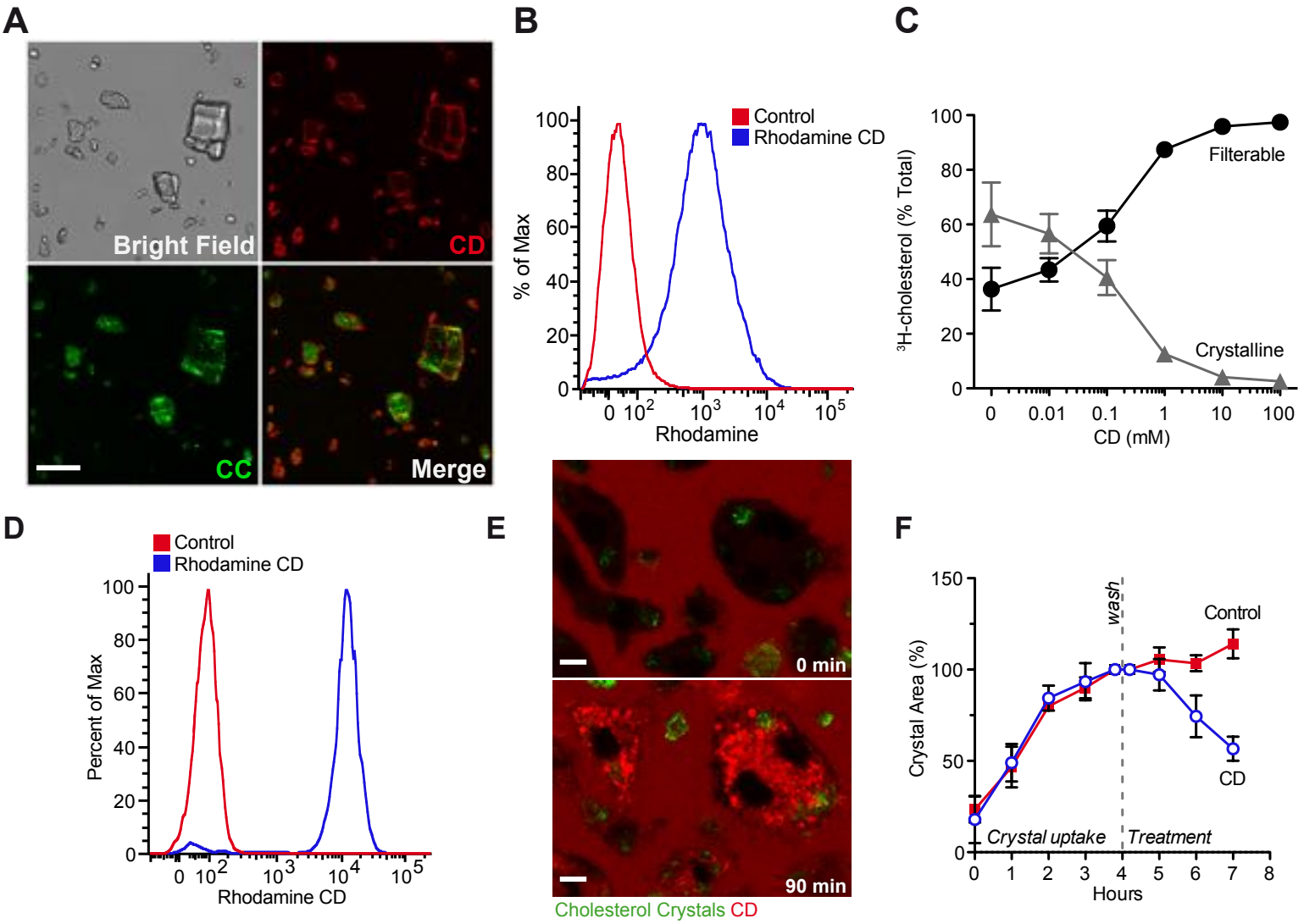
A
Bright Field
CD
CC
Merge
B
Control
Rhodamine CD
% of Max
Rhodamine
C
Filterable
Crystalline
³H-cholesterol (% Total)
CD (mM)
D
Control
Rhodamine CD
Percent of Max
Rhodamine CD
E
0 min
90 min
Cholesterol Crystals CD
F
wash
Control
CD
Crystal uptake
Treatment
Crystal Area (%)
Hours

## Figure 4

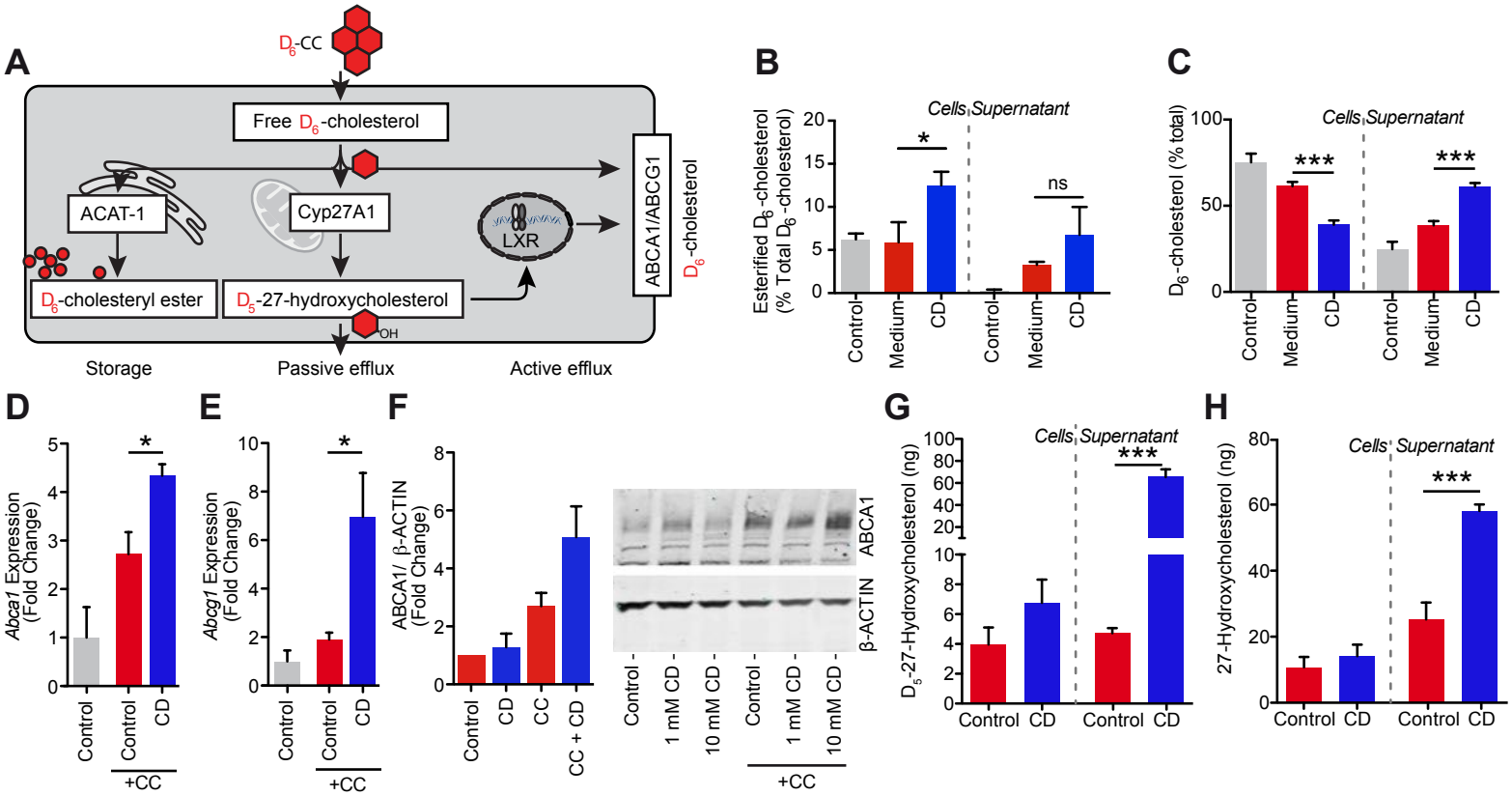
A
D6-CC
Free D6-cholesterol
ACAT-1
Cyp27A1
LXR
ABCA1/ABCG1
D6-cholesterol
D6-cholesteryl ester
D5-27-hydroxycholesterol
OH
Storage
Passive efflux
Active efflux
B
Esterified D6-cholesterol (% Total D6-cholesterol)
Cells
Supernatant
*
ns
Control
Medium
CD
C
D6-cholesterol (% total)
***
D
Abca1 Expression (Fold Change)
+CC
E
Abcg1 Expression (Fold Change)
F
ABCA1/ β-ACTIN (Fold Change)
CC
CC + CD
1 mM CD
10 mM CD
ABCA1
β-ACTIN
G
D5-27-Hydroxycholesterol (ng)
H
27-Hydroxycholesterol (ng)

**Figure 5**

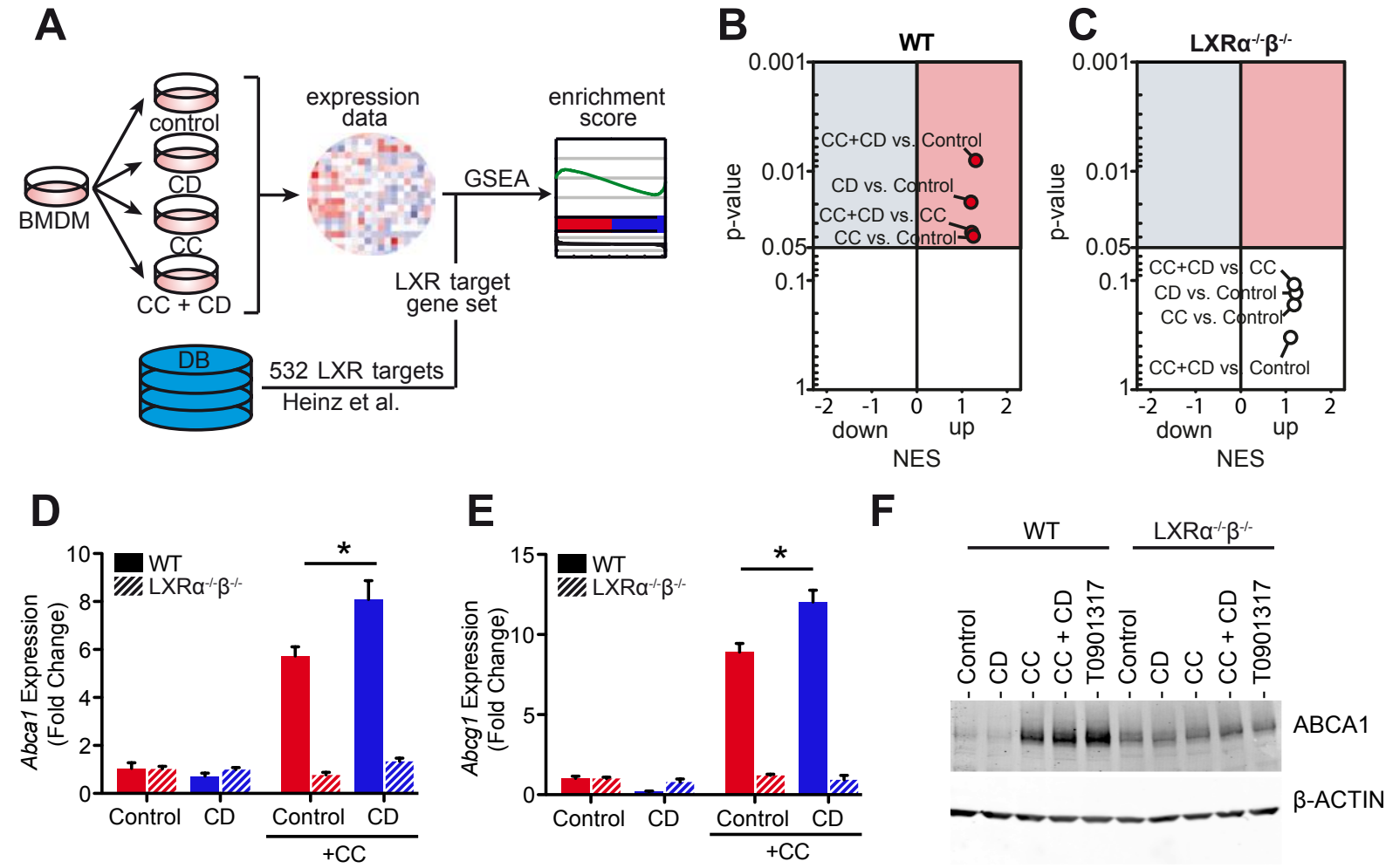
A
BMDM
control
CD
CC
CC + CD
expression data
GSEA
enrichment score
LXR target gene set
DB
532 LXR targets
Heinz et al.
B
WT
p-value
CC+CD vs. Control
CD vs. Control
CC+CD vs. CC
CC vs. Control
down
up
NES
C
LXRα-/-β-/-
CC+CD vs. CC
CD vs. Control
CC vs. Control
CC+CD vs. Control
D
Abca1 Expression (Fold Change)
WT
LXRα-/-β-/-
Control
CD
+CC
E
Abcg1 Expression (Fold Change)
F
WT
LXRα-/-β-/-
Control
CD
CC
CC + CD
T0901317
ABCA1
β-ACTIN

# Figure 6

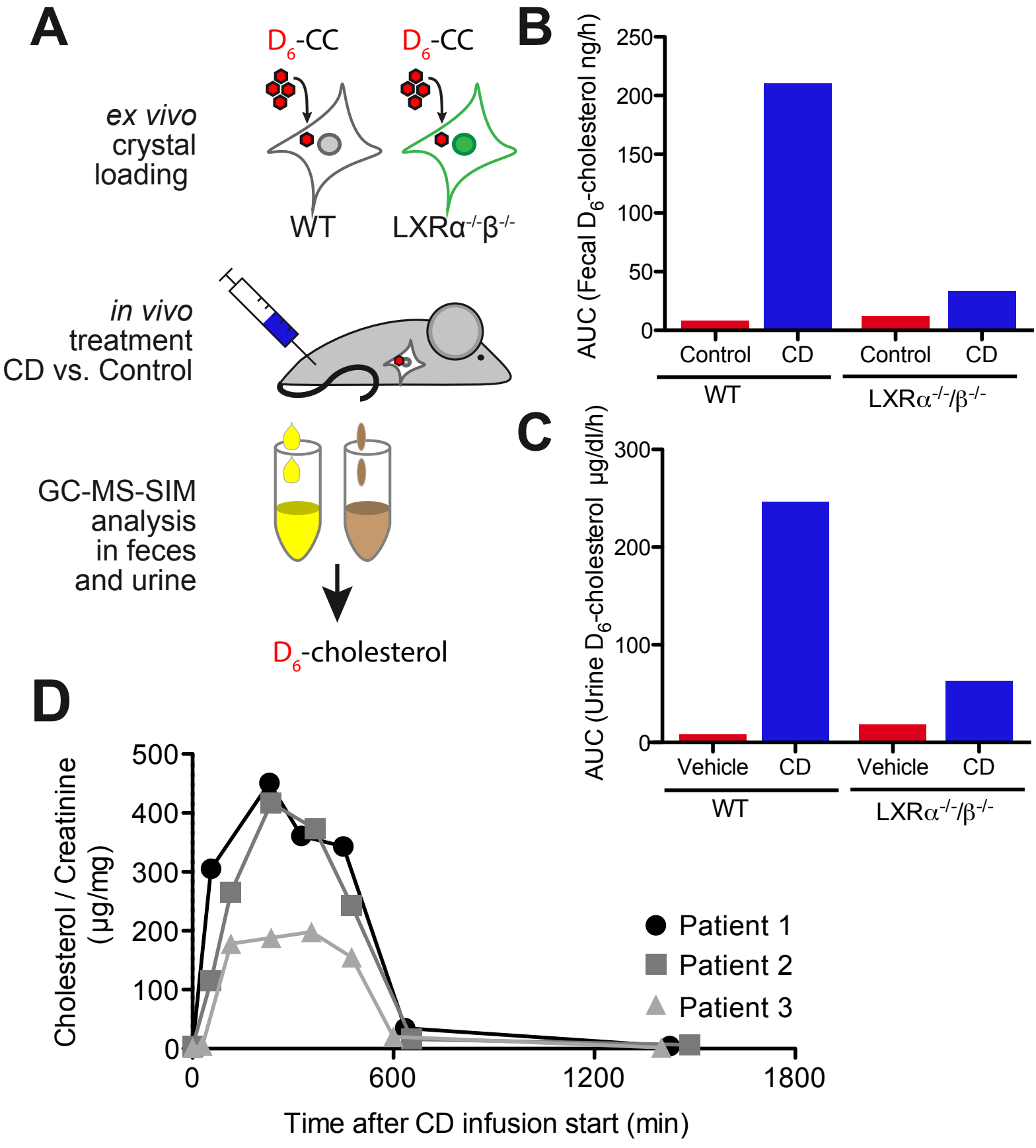
A
D6-CC
D6-CC
ex vivo
crystal
loading
WT
LXRα-/-β-/-
in vivo
treatment
CD vs. Control
GC-MS-SIM
analysis
in feces
and urine
D6-cholesterol
B
AUC (Fecal D6-cholesterol ng/h)
250
200
150
100
50
0
Control
CD
Control
CD
WT
LXRα-/-/β-/-
C
AUC (Urine D6-cholesterol µg/dl/h)
300
200
100
0
Vehicle
CD
Vehicle
CD
WT
LXRα-/-/β-/-
D
Cholesterol / Creatinine
(µg/mg)
500
400
300
200
100
0
0
600
1200
1800
Time after CD infusion start (min)
Patient 1
Patient 2
Patient 3

# Figure 7

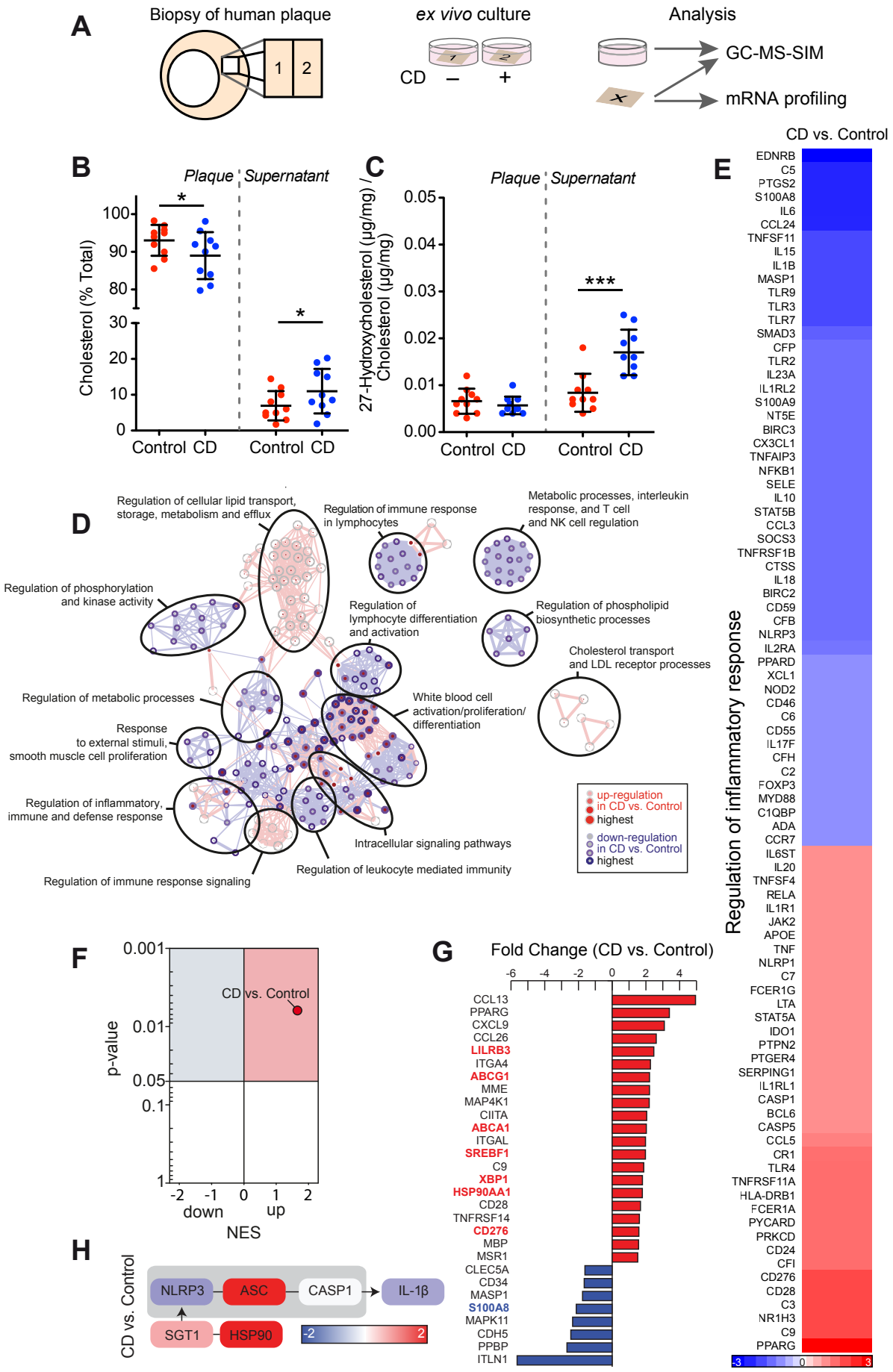
A
Biopsy of human plaque
1
2
ex vivo culture
CD – +
Analysis
GC-MS-SIM
mRNA profiling
B
Plaque
Supernatant
Cholesterol (% Total)
Control CD
Control CD
C
Plaque
Supernatant
27-Hydroxycholesterol (µg/mg) / Cholesterol (µg/mg)
Control CD
Control CD
D
Regulation of cellular lipid transport, storage, metabolism and efflux
Regulation of immune response in lymphocytes
Metabolic processes, interleukin response, and T cell and NK cell regulation
Regulation of phosphorylation and kinase activity
Regulation of lymphocyte differentiation and activation
Regulation of phospholipid biosynthetic processes
Cholesterol transport and LDL receptor processes
Regulation of metabolic processes
White blood cell activation/proliferation/ differentiation
Response to external stimuli, smooth muscle cell proliferation
Regulation of inflammatory, immune and defense response
Intracellular signaling pathways
Regulation of leukocyte mediated immunity
Regulation of immune response signaling
up-regulation in CD vs. Control highest
down-regulation in CD vs. Control highest
E
CD vs. Control
Regulation of inflammatory response
EDNRB
C5
PTGS2
S100A8
IL6
CCL24
TNFSF11
IL15
IL1B
MASP1
TLR9
TLR3
TLR7
SMAD3
CFP
TLR2
IL23A
IL1RL2
S100A9
NT5E
BIRC3
CX3CL1
TNFAIP3
NFKB1
SELE
IL10
STAT5B
CCL3
SOCS3
TNFRSF1B
CTSS
IL18
BIRC2
CD59
CFB
NLRP3
IL2RA
PPARD
XCL1
NOD2
CD46
C6
CD55
IL17F
CFH
C2
FOXP3
MYD88
C1QBP
ADA
CCR7
IL6ST
IL20
TNFSF4
RELA
IL1R1
JAK2
APOE
TNF
NLRP1
C7
FCER1G
LTA
STAT5A
IDO1
PTPN2
PTGER4
SERPING1
IL1RL1
CASP1
BCL6
CASP5
CCL5
CR1
TLR4
TNFRSF11A
HLA-DRB1
FCER1A
PYCARD
PRKCD
CD24
CFI
CD276
CD28
C3
NR1H3
C9
PPARG
F
p-value
CD vs. Control
down
up
NES
G
Fold Change (CD vs. Control)
CCL13
PPARG
CXCL9
CCL26
LILRB3
ITGA4
ABCG1
MME
MAP4K1
CIITA
ABCA1
ITGAL
SREBF1
C9
XBP1
HSP90AA1
CD28
TNFRSF14
CD276
MBP
MSR1
CLEC5A
CD34
MASP1
S100A8
MAPK11
CDH5
PPBP
ITLN1
H
CD vs. Control
NLRP3
ASC
CASP1
IL-1β
SGT1
HSP90

# Figure 8

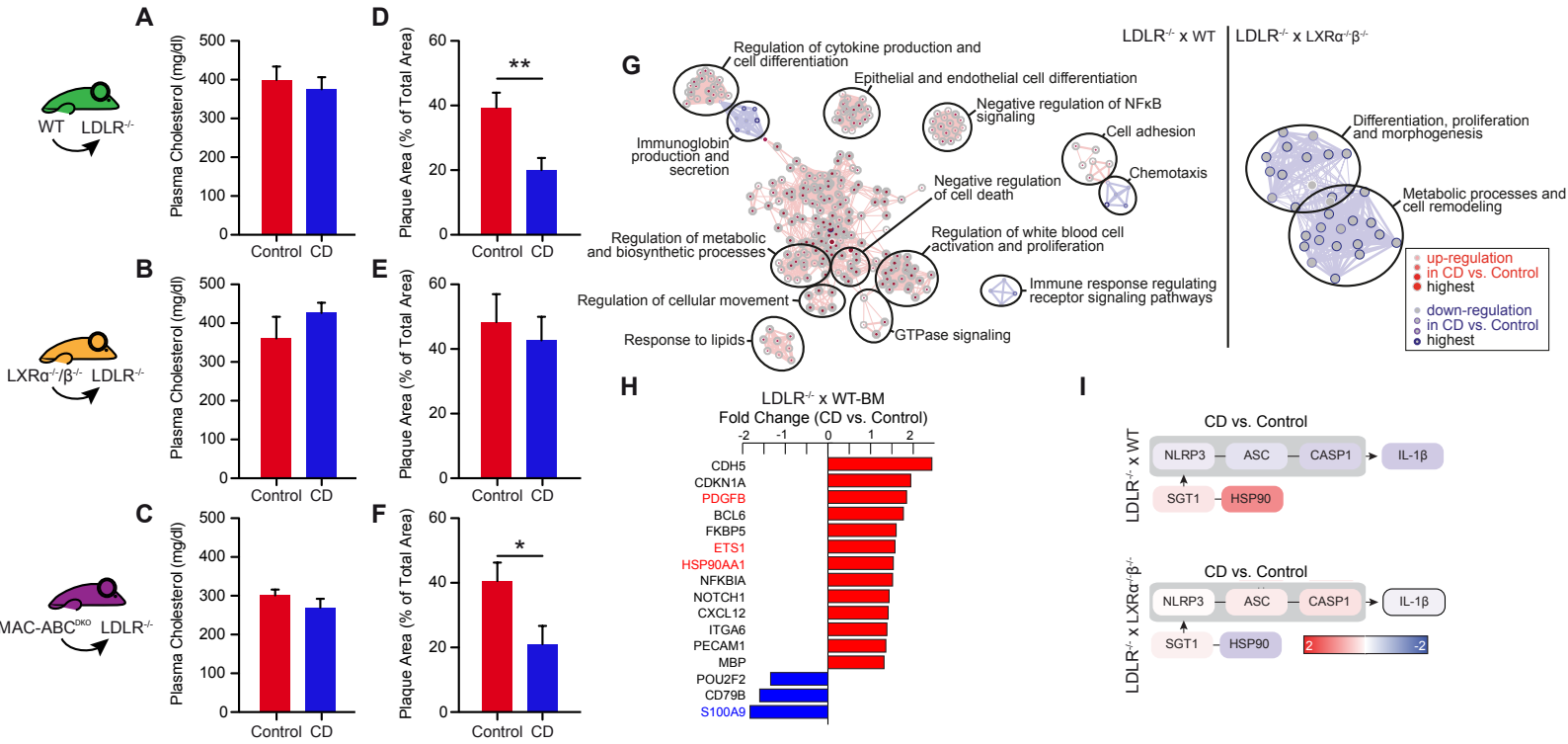
A
B
C
D
E
F
G
H
I
WT LDLR-/-
LXRα-/-β-/- LDLR-/-
MAC-ABCDKO LDLR-/-
Plasma Cholesterol (mg/dl)
Plaque Area (% of Total Area)
Control CD
**
*
LDLR-/- x WT
LDLR-/- x LXRα-/-β-/-
Regulation of cytokine production and cell differentiation
Epithelial and endothelial cell differentiation
Negative regulation of NFκB signaling
Cell adhesion
Chemotaxis
Immunoglobin production and secretion
Negative regulation of cell death
Regulation of metabolic and biosynthetic processes
Regulation of white blood cell activation and proliferation
Regulation of cellular movement
Immune response regulating receptor signaling pathways
Response to lipids
GTPase signaling
Differentiation, proliferation and morphogenesis
Metabolic processes and cell remodeling
up-regulation in CD vs. Control highest
down-regulation in CD vs. Control highest
LDLR-/- x WT-BM
Fold Change (CD vs. Control)
CDH5
CDKN1A
PDGFB
BCL6
FKBP5
ETS1
HSP90AA1
NFKBIA
NOTCH1
CXCL12
ITGA6
PECAM1
MBP
POU2F2
CD79B
S100A9
CD vs. Control
NLRP3
ASC
CASP1
IL-1β
SGT1
HSP90

**Supplementary Materials:**

## Materials and Methods:

*Study design*

The main objective of our study was to investigate whether CD exhibits atheroprotective effects and to identify the main mechanisms by which they are mediated. For this, we used murine models of atherosclerosis, studied macrophage biology *in vitro,* and performed *ex vivo* experiments with human atherosclerotic plaques. Specific details of the individual experiments are described below.

*ApoE$^{-/-}$ atherosclerosis mouse models*

12-week old ApoE$^{-/-}$ mice (Charles River) on a C57BL/6J background were used for all studies. Animals were maintained in a 22 °C room with a 12 h light/dark cycle and received chow and drinking water ad libitum.

*CD prevention protocol:* ApoE$^{-/-}$ mice were fed a cholesterol-rich diet containing 21 % fat, 19.5 % casein, and 1.25 % cholesterol for 8 weeks (Ssniff, Soest). During this time, the mice were subcutaneously injected with 2 g CD/ kg body weight or 200 µl 0.9 % NaCl as vehicle control twice a week.

*CD regression protocol:* ApoE$^{-/-}$ mice were first fed a cholesterol-rich diet for 8 weeks so that advanced atherosclerotic lesions could develop. The diet was then switched to normal chow for another 4 weeks. During these 4 weeks, the mice were concomitantly treated with either CD or 200 µl 0.9 % NaCl as vehicle control as described above.

*CD treatment protocol:* ApoE$^{-/-}$ mice were fed a cholesterol-rich diet for a total of 12 weeks. CD or vehicle control treatment was started after 8 weeks as described above.

Body weights were measured weekly. Arterial blood pressure and heart rate were assessed with a computerized tail-cuff method (CODA 6, Kent Scientific) before and after treatment. The mice were sacrificed by cervical dislocation after the indicated treatments, and tissue samples and blood were collected immediately. All animal experiments were performed in accordance with institutional guidelines and the German animal protection law.

*Bone marrow transplantation model*

Bone marrow was obtained from 14-18 week old donor mice: WT C57BL/6J, LXR$\alpha^{-/-}\beta^{-/-}$ (mixed genetic background on C57BL/6J and 129/Sv strains), and MAC-ABC$^{DKO}$ (LysmCreAbca1fl/flAbcg1fl/fl on C57BL/6J background). Donor bone marrow was collected by flushing femurs and tibiae with DMEM cell culture medium using a 23G needle. The suspension was filtered with a sterile 70 µm nylon cell strainer, and the cells were subsequently washed twice with Hank's acid citrate dextrose solution and resuspended in PBS. For full engraftment of donor bone marrow, recipient LDLR$^{-/-}$ mice on a C57BL/6J background were subjected to lethal

irradiation with 6x6 Gy over 4 hours from a OB 29/4 (Cs-137). 4 hours after irradiation, $1x10^7$ cells from donor mice were injected intravenously via a tail vein. All mice received drinking water spiked with ciprofloxacin 0.1 mg/ml for seven days to prevent systemic infection during neutropenia. The atherosclerosis trials were initiated four weeks after irradiation. All mice were fed a cholesterol-rich diet and concomitantly treated with CD or vehicle control for eight weeks as described above.

*Histological analysis of murine atherosclerotic plaques*

Hearts with ascending aortas were embedded in Tissue Tek OCT embedding medium (Miles), snap-frozen, and stored at -80°C. Samples were sectioned on a Leica cryostat (5 µm), starting at the aortic arch and progressing through the aortic valve area into the heart, and were placed on slides. For the detection of atherosclerotic lesions, aortic cryosections were fixed with 3.7% formaldehyde for 1 hour, rinsed with deionized water, stained with Oil Red O working solution (0.5%) for 30 min, and rinsed again. Hematoxylin staining was performed according to standard protocols. All sections were examined under a Zeiss Axiovert 200M microscope using AxioVision software. For quantification of atherosclerotic plaque formation in the aortic root, lesion area and total area of 3-4 serial histological sections of the aortic root were quantified for each mouse. Atherosclerosis data are expressed as plaque area in percent of total vessel wall area. For analysis of cholesterol crystal plaque load, aortic cryosections were fixed with 4% paraformaldehyde for 30 min at 21°C. They were then blocked and permeabilized with 5% fetal calf serum, 5% bovine serum albumin, 10% normal goat serum, and 0.1% saponin in PBS for 60 min at 21°C. The primary rat anti-mouse CD68 antibody (MCA1957, AbD Serotec) was diluted to 2 µg/ml in 10% normal goat serum/ PBS, and the slides were incubated overnight at 4°C. The secondary goat anti-rat IgG Alexa647 conjugate (Invitrogen) was diluted to 4 µg/ml in 10% normal goat serum/ PBS, and the slides were incubated for 60 min in the dark at 21°C. The sections were again washed 3x with 10% normal goat serum/ PBS and subsequently counterstained with Hoechst 33342 (Immunochemistry) diluted to 5 µg/ml in PBS for 2 min in the dark at 21°C. Coverslips were mounted with 80% glycerol and the edges carefully sealed with a quick-drying two-component epoxy adhesive.

*Confocal laser reflection and fluorescence microscopy*

Confocal microscopy was performed with a Leica TCS SP5 II AOBS confocal laser-scanning microscope. Immunofluorescence staining was detected by standard confocal imaging techniques, and CCs were visualized by laser reflection microscopy as previously described *(5, 42)*. In brief, the detector and the acousto-optical beam splitter were set to allow the detection of reflected laser light. Plaque CC content was quantified from 3-4 sections per mouse using Volocity Quantitation (PerkinElmer) and depicted as a ratio of total crystal reflection area to total plaque area. Investigators performing the histological analyses were blinded to the treatment of the respective animals.

*Measurement of reactive oxygen species*

ROS release in intact aortic segments was determined by L-012 chemiluminescence. Aortic segments of the proximal descending aorta just distal to the ostium of the left subclavian artery were carefully excised and placed in chilled, modified Krebs-HEPES buffer (pH 7.4) composed

of NaCl 99.01 mM, KCl 4.69 mM, $CaCl_2$ 1.87 mM, $MgSO_4$ 1.20 mM, Na-HEPES 20.0 mM, $K_2HPO_4$ 1.03 mM, $NaHCO_3$ 25.0 mM, and D(+)glucose 11.1 mM and contained additional ascorbic acid (0.28 mM) and indomethacin (0.01 mM) *(43)*. Connective tissue was removed and aortas were cut into 2 mm segments. Chemiluminescence of aortic segments was assessed in scintillation vials containing the modified Krebs-HEPES buffer with 100 µmol/l L-012 over 15 min in a scintillation counter (Lumat LB 9501, Berthold) in 1 min intervals. The vessel segments were then dried and dry weight was determined. ROS release was calculated as relative chemiluminescence per mg aortic tissue.

*Quantification of plasma cholesterol, precursors and phytosterols*

Plasma concentration of cholesterol was measured by GC-flame ionization detection using 5α-cholestane as internal standard. Cholesterol precursors such as lathosterol, lanosterol, dihydro-lanosterol, and desmosterol, together with the cholesterol 5α -saturated metabolite 5α-cholestanol and the phytosterols campesterol, sitosterol, and stigmasterol were quantified by GC-MS-SIM, using epicoprostanol as internal standard *(44, 45)*. Cholesterol precursors were used as surrogate markers of cholesterol synthesis. 5α-cholestanol and plant sterols indicate sterol uptake/absorption.

*Isolation of plasma lipoproteins by FPLC*

For lipoprotein separation by fast performance liquid chromatography (FPLC), total plasma cholesterol concentrations were first determined with the Infinity Cholesterol Liquid Stable Reagent (Thermo Fisher Scientific). After that, a 50 µl serum aliquot was pre-warmed to 37°C for 5 min and then filtered through a PVDF 0.45 µm membrane filter. The filtered samples (20 µl each) were subsequently fractionated by FPLC gel filtration on a Superose 6 PC 3.2 /30 column at 4°C (GE Healthcare). The elution fractions were monitored using absorbance at 280 nm with a constant flow of 40 µl/min, and fractions (40 µl) were collected beginning 18 min after sample injection. Cholesterol in each fraction was measured using the enzymatic cholesterol assay, and the area under the curve for VLDL, LDL, and HDL was determined in comparison to a standard of known amounts of human VLDL, LDL, and HDL run in parallel.

*Flow cytometry*

Murine blood samples were analyzed as previously described *(46)*. After red blood cell lysis, the viable lymphocyte population was analyzed for sca-1-FITC (Becton Dickinson) and flk-1-PE (Becton Dickinson). Isotype identical antibodies (Becton Dickinson) and unstained samples served as controls in every experiment. Cell fluorescence was measured immediately after staining using a FACSCalibur instrument (Becton Dickinson). Data were analyzed using CellQuest software (Becton Dickinson). Units of all measured components are specific events detected after measuring 20,000 events in a pre-specified lymphocyte gate during FACS analysis. Relative lymphocyte, monocyte, and granulocyte counts were determined using predefined gates.

*Cholesterol crystal preparation*

CCs were prepared from a 2 mg/ml cholesterol solution in 1-propanol. Crystallization was induced by addition of 1.5 volumes of endotoxin-free water. CCs were dried and resuspended in sterile PBS.

*Cell Culture*

Cells were cultured at 37°C, 5% $CO_2$ in a humidified atmosphere. BMDMs were derived from bone marrow isolated from tibiae and femurs of LXR$\alpha^{-/-}\beta^{-/-}$ mice (mixed genetic background on C57BL/6J and 129/Sv strains) and age and gender matched WT C57BL/6J mice. Bone marrow cells were cultured in DMEM supplemented with 10 % FCS, 10 µg/ml Ciprobay-500, and 40 ng/ml M-CSF (R&D Systems) for six days. Immortalized mouse macrophages from WT C57BL/6J mice (iMacs) were cultured in DMEM supplemented with 10% fetal calf serum (FCS) and 10 µg/ml Ciprobay-500 (Bayer).

*CD binding and uptake assays*

To assess CD binding to CCs, 1 mg CCs were incubated in 0.5 mM RBITC-NH2-HPβCD (rhodamine CD, Cyclolab) for 6 hours at room temperature (RT). Crystals were washed 5x with PBS before confocal microscopic or flow cytometric analyses. For investigation of cellular CD uptake, iMacs were incubated with 20 µg CCs for 3 hours. For confocal microscopic analysis, living cells were imaged for 6 hours after addition of 1 mM rhodamine CD mixed with unlabeled CD in a 1:10 ratio. Uptake was saturated after 2 hours. For flow cytometric analysis, CC-loaded macrophages were incubated for 3 hours in a 1 mM CD solution containing rhodamine CD and unlabeled CD in a 1:10 ratio. After washes with PBS, the cells were harvested, and intracellular rhodamine fluorescence was detected with a MACSQuant analyzer (Miltenyi Biotec). Data were analyzed with FlowJo.

*Cell viability assay*

Cell viability was determined by incubating cells in CellTiter-Blue reagent (Promega) at 37 °C for up to 2 hours before fluorescence was measured according to the manufacturer's instructions. Untreated cells served as positive control and 70 % ethanol-treated cells were used as negative control (dead cells).

*Radioactive cholesterol crystal dissolution assay*

Radioactively labeled CCs were prepared from a 2 mg/ml cholesterol solution composed of 0.1 mCi [1,2-$^3$H]-cholesterol (Perkin Elmer) in a 1:50 (w/w) ratio with unlabeled cholesterol (Sigma) as described above. After crystallization, the crystal solution was filtered through a 0.22 µm spin filter column to remove free [1,2-$^3$H]-cholesterol. CCs were recovered from the filter membrane and incubated overnight, shaking at 37°C in CD solutions of indicated concentrations. Filtration through 0.22 µm filter plates was used to determine the amount of solubilized [1,2-$^3$H]-cholesterol in the filtrate. The retentate was washed and subsequently incubated in ethanol for 2 hours to quantify the amount of total crystalline [1,2-$^3$H]-cholesterol.

*Polarization microscopy of intracellular cholesterol crystal dissolution*

iMacs were incubated with 20 µg CCs for 4 hours, washed with PBS, and then incubated with 10 mM CD or medium control for another 3 hours. Polarization images of the cells were acquired every 60 min. Crystal area was assessed by automated image analysis with Zeiss AxioVision software. Data are presented as percentage of the crystal area immediately after.

*Lipid droplet staining*

iMacs were incubated with 20 µg CCs for 3 hours, washed with PBS, and fixed with 4% paraformaldehyde for 30 min at RT. For LD540 staining, cells were stained with 1 µg/ml fluorochrome-conjugated cholera toxin subunit B (Invitrogen) for 10 min and LD540 *(47)* diluted to 0.1 µg/ml in PBS for 30 min at RT. For Oil Red O staining, the slides were quickly rinsed with 60% isopropanol and stained with 0.4% Oil Red O working solution (60% isopropanol) for 30 min at RT. A counterstain with hematoxylin was performed according to standard protocols.

*Analysis of crystal-derived cholesterol in macrophages*

Isotope-labeled CCs were prepared from [26.26.26.27.27.27-$^{2}H_6$]-Cholesterol ($D_6$-cholesterol, CDN isotopes) as described above. iMacs were incubated for 3 hours with 200 µg $D_6$-CCs/ $1x10^6$ cells. Extracellular $D_6$-CCs were washed away, and a control sample was harvested to assess the D6-cholesterol distribution before further treatment. The remaining cells were treated for 24 hours (cholesterol efflux analysis) or 48 hours (cholesterol ester and oxysterol measurements) with 10 mM CD. Supernatant and cell fractions were harvested, and free sterols and oxysterols were extracted and analyzed by GC-MS-SIM.

*Gas chromatographic-mass spectrometric-selected ion monitoring*

Degree of esterification of $D_6$-cholesterol after uptake of $D_6$-CC into macrophages was calculated from the difference of the concentrations with (total $D_6$-cholesterol) and without (free $D_6$-cholesterol only) alkaline hydrolysis in cells and supernatants. After extraction of $D_6$-cholesterol and derivatization to its trimethyl (TMSi) silylether, we performed GC-MS-SIM with epicoprostanol as internal standard on m/z 464 [$M^+$] for the TMSi ether of $D_6$-cholesterol and m/z 370 [$M^+$] for epicoprostanol *(48)*. The oxidized metabolite [26.26.26.27.27-$^{2}H_5$](25R)-26-Hydroxycholesterol ($D_5$-27-hydroxycholesterol) was determined from the same fractions by GC-MS-SIM on m/z 461 [$M^+$-90]. Authentic cholesterol and its oxidation product 27-hydroxycholesterol were measured by GC-MS-SIM on m/z 458 [$M^+$] and m/z 456 [$M^+$-90], respectively *(49)*.

*In vivo model of CC-derived reverse cholesterol transport*

16-week old C57BL/6J mice were intraperitoneally injected with $15x10^6$ BMDMs from WT or LXR$\alpha^{-/-}\beta^{-/-}$ mice that were incubated with 100 µg $D_6$-CCs/$1x10^6$ cells for 3 hours before injection. Mice were then subcutaneously injected with 2 g CD/ kg body weight or 200 µl 0.9 % NaCl as vehicle control. Feces and urine were collected every 3 hours for 30 hours, and the pooled samples were analyzed for crystal-derived $D_6$-cholesterol with GC-MS-SIM. For the depiction of fecal $D_6$-cholesterol, we used the ratio area of $D_6$-cholesterol to 5α-cholestane. The results are

presented as area under the curve of the amount of excreted $D_6$-cholesterol per time after CD injection.

*Quantitative reverse-transcriptase PCR*

For cellular gene expression analysis, macrophages were incubated for 3 hours with 100 µg CCs/ $1x10^6$ cells and treated for 4 hours with 10 mM CD before the cells were disrupted with a 10 G needle. For assessment of vascular gene expression, mouse aortas were excised, quickly frozen in liquid nitrogen, and homogenized with a motorized homogenizer in Trizol. RNA was isolated with peqGOLD RNA-Pure (peqLAB Biotechnology) according to the manufacturer's protocol, then purified with the RNeasy MiniElute cleanup kit (Qiagen). Total RNA was quantified by UV spectroscopy at 260 nm. The quality of the isolated RNA samples was determined by measuring the A260/A280 ratio, and the integrity of the ribosomal 28S and 18S bands was determined by agarose-gel electrophoresis. Then, 1 µg of the isolated total RNA was reverse transcribed with the Omniscript RT Kit (Qiagen) according to the manufacturer's protocol. The single-stranded cDNA was amplified by real-time quantitative reverse transcription-polymerase chain reaction with the TaqMan system using commercially available Taqman probes (*Abca1* Mm00442646_m1, *Abcg1* Mm00437390_m1, Applied Biosystems). *Abca*1 and *Abcg*1 mRNA expression was normalized to 18S (Mm03928990_g1, Taqman probes, Applied Biosystems).

*Western blotting*

Macrophages were incubated for 3 hours with 100 µg CCs/ $1x10^6$ cells and treated for 24 hours with 10 mM CD. LXR agonist T0901317 (Sigma) was used as a positive control for LXR activation. Cells were lysed on ice for 30 min with 1x RIPA buffer (20 mM Tris-HCl pH 7.4, 150 mM NaCl, 1 mM EDTA, 1% Triton X-100, 10% glycerol, 0.1% SDS, 0.5% deoxycholate, 0.1 µM PMSF) supplemented with complete protease inhibitors (Roche Biochemicals). Protein concentrations were determined by BCA assay (Pierce), and equal amounts of protein were loaded on 4-12% pre-cast SDS-PAGE gels (Novex, Invitrogen) with MOPS running buffer (Novex, Invitrogen). Proteins were transferred to PVDF membranes (Millipore), and membranes were blocked in 3% BSA in TBS with Tween-20, incubated with mouse monoclonal ABCA1 antibody (MAB10005, Millipore) and rabbit monoclonal β-actin antibody (Li-Cor Biosciences) overnight at 4°C. The membranes were washed and incubated with secondary anti-mouse and anti-rabbit antibodies (Li-Cor Biosciences) for 45 min in the dark. Immunoreactivity was visualized by near-infrared detection (Odyssey, LICOR).

*Gene expression profiling by Illumina Bead Chip technology*

Biotin-labeled cRNA was generated using the TargetAmp Nano-g Biotin-aRNA Labeling Kit for the Illumina System (Epicentre). Biotin-labeled cRNA (750 ng) was hybridized to Human HT-12V3 Beadchips (Illumina) and scanned on an Illumina iScan or HiScanSQ system.

*Primary data and quality control analysis of microarray data*

Raw intensity data were processed and exported with Genome Studio V2011.1 (Copyright 2003-2011 Illumina). All array data were imported into Partek Genomics Suite version 6.6 (PGS,

Copyright 2012 Partek Incorporated). Quality control assessments, including principle component analysis and box-whisker plots to visualize expression distribution, were applied.

*Bioinformatic analysis of microarray data*

Non-normalized data (log2) were quantile normalized, and transcripts with variable expression within the dataset as well as differentially expressed (DE) genes between the different conditions were calculated using two-way ANOVA models including batch correction sentrix bar code and gender where applicable. For analyses of the microarray data on BMDMs derived from WT or LXR$\alpha^{-/-}\beta^{-/-}$ mice (GSE67013), DE genes were defined by a fold change (FC) greater than 2 and p-value<0.05. Gene Set Enrichment Analysis (GSEA) was used to determine whether a defined set of genes is statistically significant between two different states. A set of genes was considered to be statistically significantly enriched when the p-value was $\leq 0.05$ and the false discovery rate (FDR) was $\leq 0.25$ comparing two different states. GSEA was performed with 1000 permutations against a list of LXR target genes generated from the LXR target genes identified by Heinz *et al. (30)* (Table S1). For analyses of the microarray data on descending aortas of mice from the bone marrow transplantation model (GSE67011), DE genes were defined by a FC greater than 1.3 and p-value<0.05. To link the DE genes for CD vs. control to known gene networks, we performed Gene Ontology Enrichment Analysis (GOEA) using the Cytoscape (http://www.cytoscape.org/) plug-in BiNGO (v2.44) *(50)*. The FDR threshold was set to 0.05 to include only significant results. The Cytoscape plugins Enrichment Map (v1.1) *(51)* and Word Cloud *(52)* were used to visualize GO networks. The cutoff for the Jaccard coefficient was set to 0.51 and the FDR q-value to 0.1. The expression of genes relevant for the NLRP3 inflammasome pathway was visualized in Partek Pathway.

*Cholesterol quantification in urine of NPC1 patients*

NPC1-deficient patients receive weekly infusions of 2000 mg CD/kg body weight over 8 hours (ClinicalTrial.gov NCT01747135). Urine samples from three individual NPC1 patients were collected at the indicated time points after starting the intravenous CD application. Urine cholesterol concentration was determined by GC-MS-SIM as described above and normalized to urine creatinine excretion. The study protocol followed procedures in accordance with the Helsinki Declaration of 1975 (revised 1983), and the I-IND (Individual-Investigative New Drug) protocol was approved by the FDA. Written informed consent was obtained from the legal guardians of all subjects.

*Patient cohort for human atherosclerotic carotid plaques*

Patients with high-grade internal carotid stenosis (≥70%) or ischemic stroke within the last month were recruited at the Department of Neurology, Oslo University Hospital Rikshospitalet. The carotid stenosis was diagnosed and classified by precerebral color duplex and CT angiography according to consensus criteria. As part of the ultrasound examination, the total extracranial part of the carotid artery was examined with B-mode and Doppler analyses. Ultrasound plaque appearance in terms of echogenicity was classified according to consensus criteria *(53)*. Exclusion criteria were heart failure, liver disease, kidney disease, and severe concomitant disease such as infection, connective tissue disease, or malignancy. The Regional Health Authorities of South-Eastern and Western Norway approved the study protocols (REK no: S-

0923a 2009/6065). The study confirms with the principles outlined in the Declaration of Helsinki for use of human tissue or subjects. Signed informed consent was obtained from all participants.

*Culturing of human atherosclerotic carotid plaques*

Biopsies from atherosclerotic carotid plaques (n=10), obtained from patients who had been suffering from symptoms within 1 month and/or had stenosis of ≥ 70%, were placed in Dulbecco's modified Eagle's medium ([D-MEM]/F12; Gibco) enriched with 30 mg/ml endotoxin-free and fatty acid-free bovine serum albumin (Sigma). The biopsies containing atherosclerotic plaques of each patient were split into two macroscopically equal pieces and incubated for 16 hours with 10 mM CD or PBS. The plaque biopsies were then split into two pieces and either placed in RNA Later (Qiagen) for RNA analysis or snap frozen for lipid analysis. Plaque supernatants were collected, centrifuged (1700 *g* for 5 min, 4°C), and snap frozen before being stored at -80°C until further analysis.

*Sterol and oxyphytosterol analyses from dried plaque tissue and supernatant*

After being excised and worked up as described before, plaque tissue was dried in a Savant SpeedVac concentrator (Thermo Fisher Scientific) for 24 hours. Cholesterol, non-cholesterol sterols, and oxysterols were extracted from dry weight aliquots using Folch reagent [chloroform/methanol 2:1 (v:v), with 0.25 mg BHT added per mL solvent] for 10 mg dried plaque tissue. Extraction was performed for 24 hours at 4°C in a dark cold room. The extracts were kept at -20°C until analysis. One ml of supernatant and one ml of the Folch extract of plaque tissue was subjected to alkaline hydrolysis, extraction of the free sterols and oxysterols, silylation to their corresponding (di)trimethylsilyl ethers, and then gas chromatographic separation and detection either by flame ionization detection (for cholesterol, using 5α-cholestane as internal standard) or by mass selective detection (for non-cholesterol sterols or oxysterols, using epicoprostanol and the corresponding deuterium-labeled oxysterols as internal standards, respectively) as described in detail previously *(45, 54)*.

*Nanostring analysis of human atherosclerotic carotid plaques*

Plaque pieces were cut into similar sizes, and homogenization was performed with a FastPrep 24 instrument (≈6 m/s, MD Biomedicals) three times for 40 seconds with zirconium oxide beads (Bertin Tech) (six 2.8 mm beads and 0.8 g 1.4 mm beads per sample) in Isol-RNA Lysis Reagent (VWR, 5Prime). The aqueous phase was isolated after adding chloroform and centrifugation (13000 rpm, 15 min, 4°C), and RNA was isolated further with RNeasy microkit (Qiagen). Nanodrop spectrophotometer (ND-1000, Saveen Werner) was used to measure RNA concentration, and 100 ng was applied from each sample for RNA expression analysis, running one strip of 12 samples at a time on a nCounter analysis system (Nanostring Technologies). The procedure was performed according to the manufacturer´s instructions. The kit used was a fixed codeset for mRNA analysis, nCounter GX Human Immunology Kit v2 (Nanostring Technologies), spiked with another 30 probes of our own choice (nCounter Panel Plus, Table S3).

*Bioinformatic analysis of Nanostring data*

The number of mRNA molecules counted was imported into NSolver with default settings, corrected, and normalized against non-detected background (mean of negative controls + 2 standard deviations) and instrumental variations (positive controls) and against the reference genes annotated in the kit that were found to be stable (RPL19, EEF1G, TUBB, OAZ1, GAPDH, POLRA2, G6PD, HPRT1) (NSolver Analysis Software 2.5.34, Nanostring Technologies). The data were further imported into Partek Genomics Suite 6.6; non-detected values were set to 1, and the data were batch-corrected for the interaction strip and patient. GSEA was performed with 1000 permutations on the dataset using a LXR target gene list generated from the direct LXR target genes identified in Pehkonen *et al. (55)* (Table S2). The result was considered statistically significantly enriched when the p-value was $\leq 0.05$ and the FDR was $\leq 0.25$ comparing two different states. DE genes calculated by three-way ANOVA were defined by a FC greater than 1.3 and p-value<0.05. To link the DE genes for CD vs. PBS to known gene networks, we performed GOEA using the Cytoscape (http://www.cytoscape.org/) plug-in BiNGO (v2.44) *(50)*. The FDR threshold was set to 0.05 to include only significant results. The Cytoscape plugins Enrichment Map (v1.1) *(51)* and Word Cloud *(52)* were used to visualize GO networks. The cutoff for the Jaccard coefficient was set to 0.51 and the FDR q-value to 0.1. The expression of genes relevant for the NLRP3 inflammasome pathway was visualized in Partek Pathway *(56, 57)*.

*Statistics*

Unless otherwise indicated, data are presented as mean ± standard error of mean (s.e.m.). For statistical analysis, we used two-tailed, unpaired Student's t-test and ANOVA for multiple comparisons. Post-hoc comparisons were performed with the Tukey test. $p<0.05$ was considered statistically significant. Original data and all significant p-values are included in Table S4. Basic analyses were performed with Excel (Microsoft) and Prism (GraphPad Software, Inc.). Furthermore, Volocity Quantitation (PerkinElmer) was used for image analysis, and gene expression data were analyzed with Partek Genomics Suite (Partek) using ANOVA models. GSEA results were plotted using Sigmaplot 12.2.

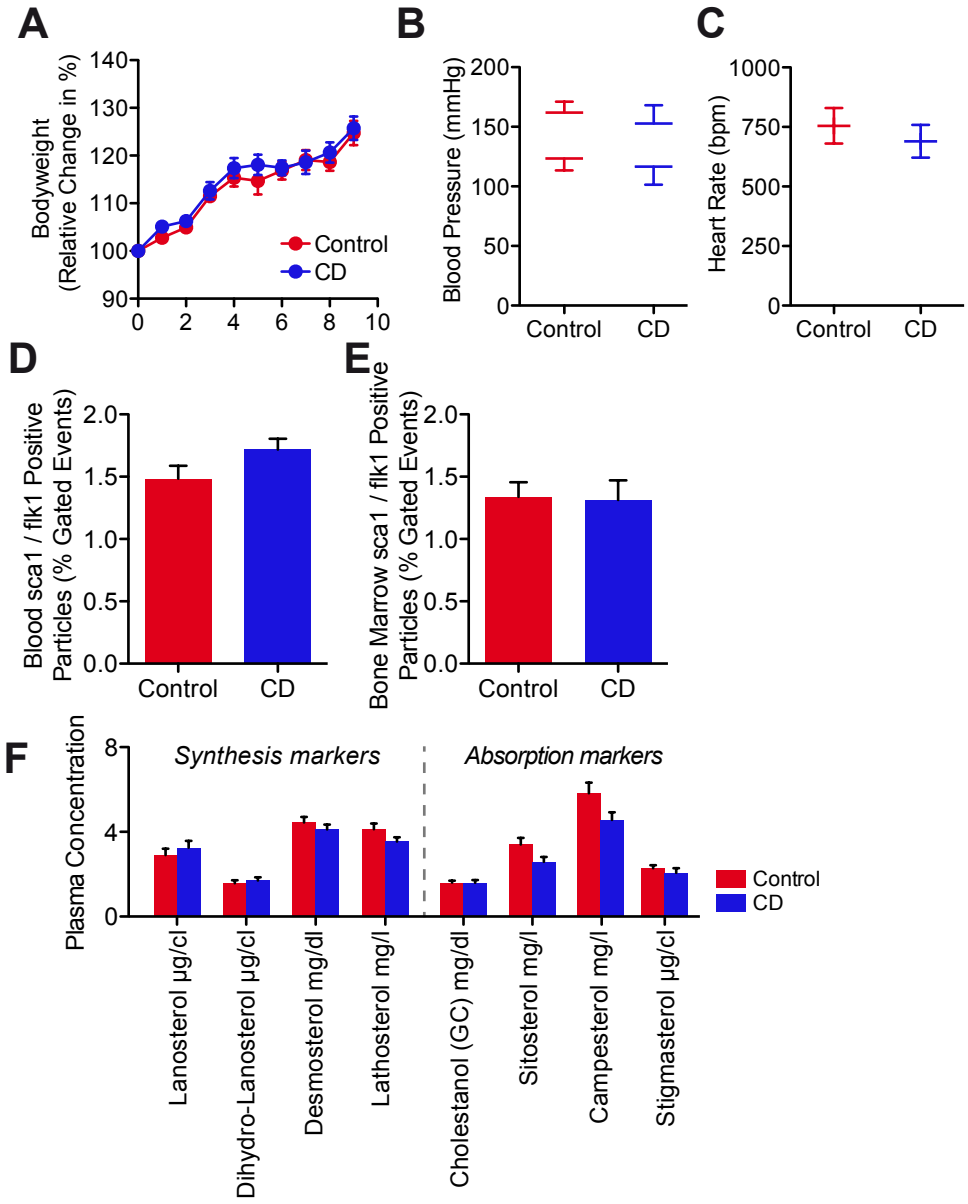


**Fig. S1. CD treatment does not influence general cardiovascular parameters.** ApoE$^{-/-}$ mice were fed a cholesterol-rich diet for eight weeks and concomitantly treated with 2 g CD/ kg body weight or vehicle control twice a week (n=7-8 per group). **(A)** Weekly change in body weight relative to starting weight. **(B)** Blood pressure and **(C)** heart rate in the final week of CD or control treatment. Percentage of **(D)** circulating and **(E)** bone marrow sca1/flk1 positive cells relative to the number of gated events. **(F)** Plasma concentration of cholesterol precursors as "synthesis markers" and the metabolite cholestanol and selected phytosterols as "absorption markers." Data are shown as mean + s.e.m. or mean +/- s.e.m.

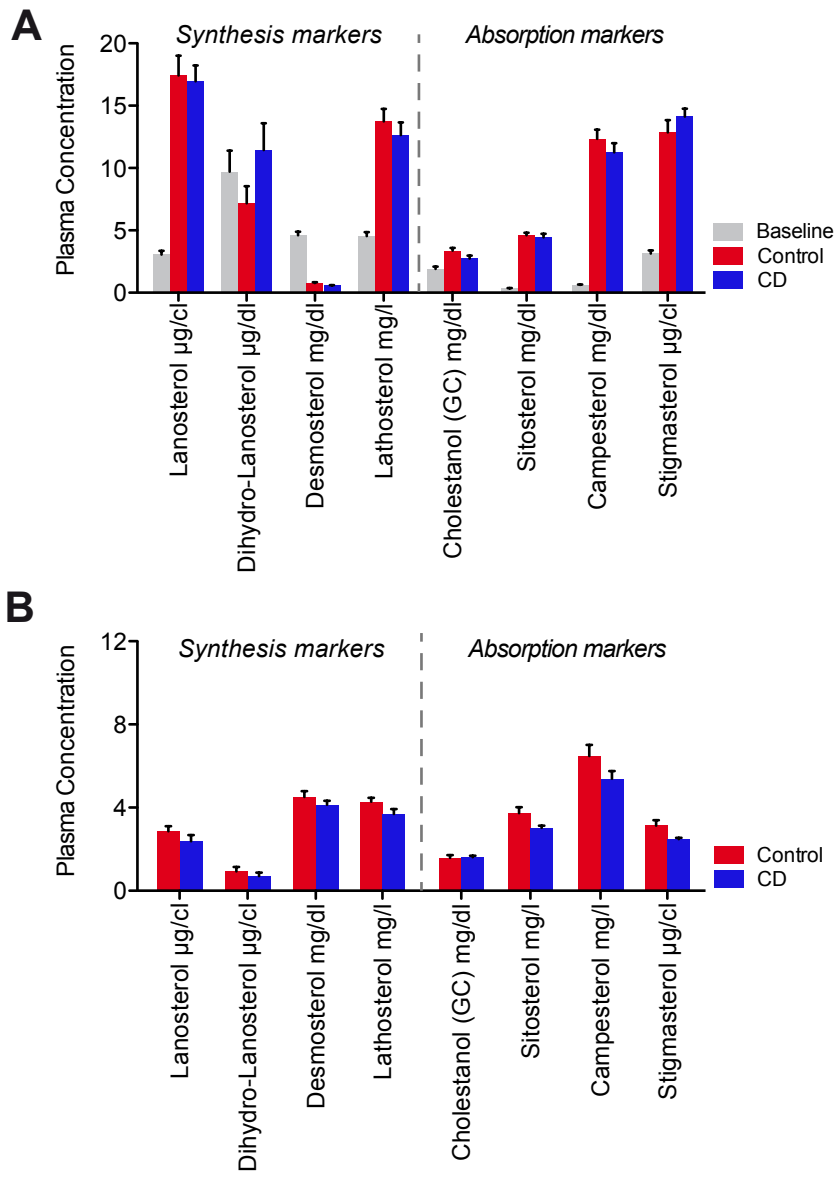


**Fig. S2. CD treatment does not alter plasma sterol concentrations in atherosclerosis regression trials.** Plasma concentration of cholesterol precursors as "synthesis markers" and the metabolite cholestanol and selected phytosterols as "absorption markers" in **(A)** regression and **(B)** treatment trials (n=4-8 per group). Data are shown as mean + s.e.m.

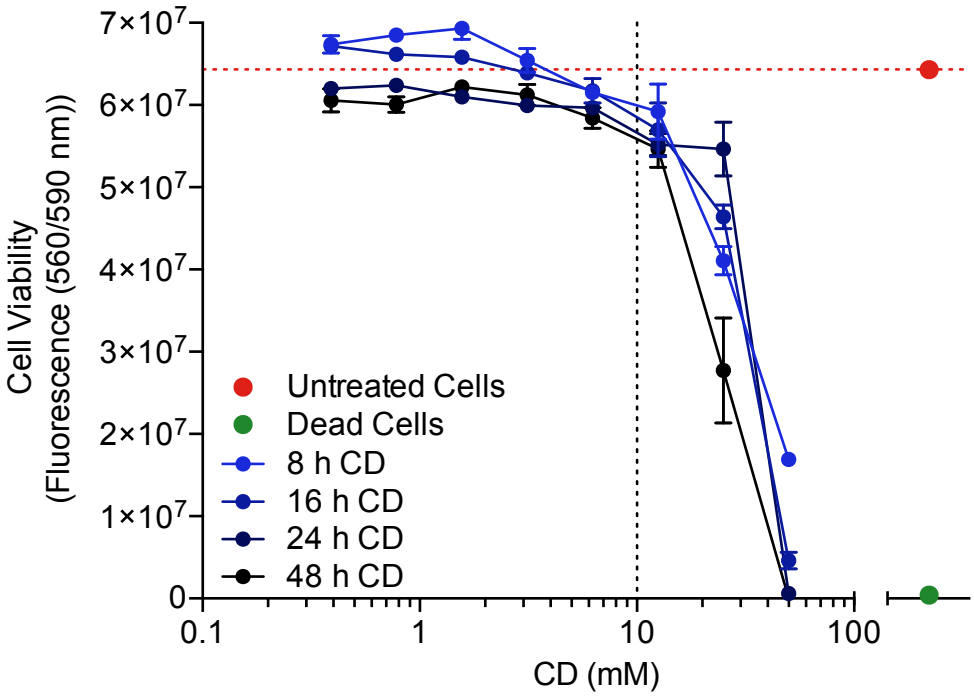


**Fig. S3. 10 mM CD does not affect the viability of murine macrophages.** Cell viability of iMacs incubated for indicated times with increasing concentrations of CD ranging from 0.391 mM to 50 mM. Dashed line indicates the commonly used CD concentration (10 mM). Data are shown as mean +/- s.e.m.

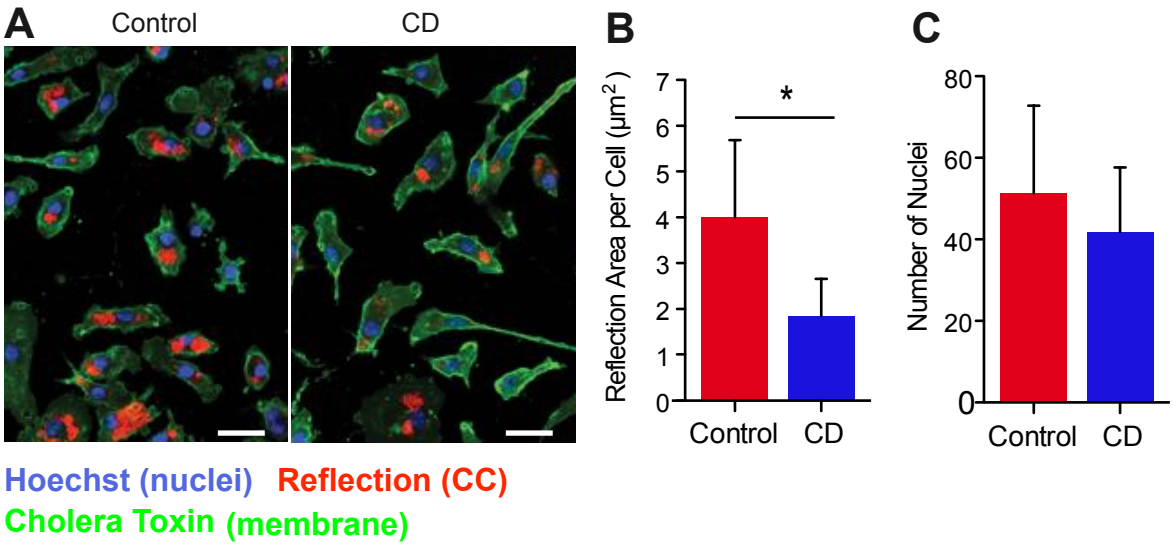


**Fig. S4. CD mediates intracellular CC dissolution.** BMDMs were loaded with 100 µg CC/1x$10^6$ cells for 3 hours and incubated with control or CD for 24 hours. (A) Representative images of CD- and control-treated cells obtained by confocal laser reflection microscopy; laser reflection signal (red), nuclei stained with Hoechst (blue), and plasma membrane stained with Alexa Fluor 647-coupled cholera toxin subunit B (green). Scale bars equal 25 µm. (B) Intracellular CC reflection signal was determined by automated image quantification based on cell mask. (C) Number of cells analyzed for intracellular CC reflection determined by number of nuclei counted. Data are shown as mean + s.e.m. Control vs. CD, unpaired one-tailed Student's t test; *$p < 0.05$.

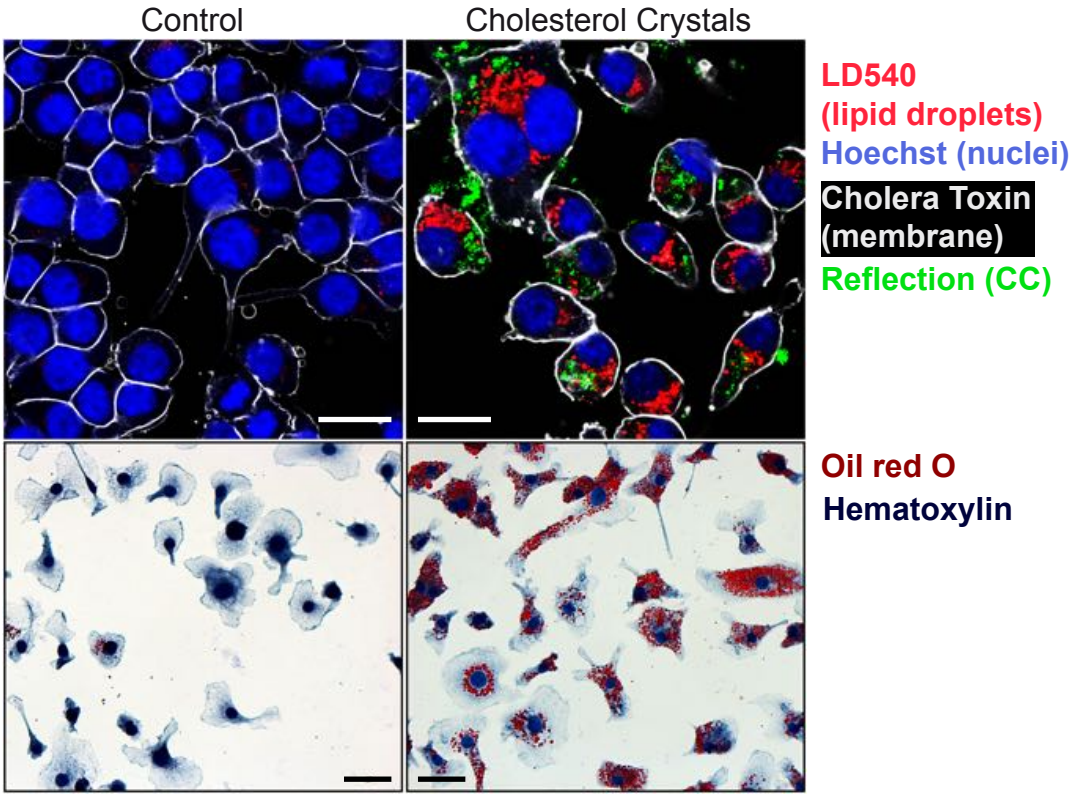


**Fig. S5. CC loading of macrophages induces lipid droplet accumulation.** iMacs were loaded with 20 μg CC for 3 hours. To visualize lipid droplet formation, resting and CC-loaded macrophages were imaged by two different staining techniques. Top: Representative images obtained by confocal laser reflection microscopy; laser reflection signal (green), lipid droplets stained with LD540 *(46)* (red), nuclei stained with Hoechst (blue), and plasma membrane stained with Alexa Fluor 647-coupled cholera toxin subunit B (white). Scale bars equal 25 μm. Bottom: Macrophages were stained for neutral triglycerides and lipids with Oil Red O (red) and counterstained with hematoxylin (dark blue). Scale bars equal 25 μm.

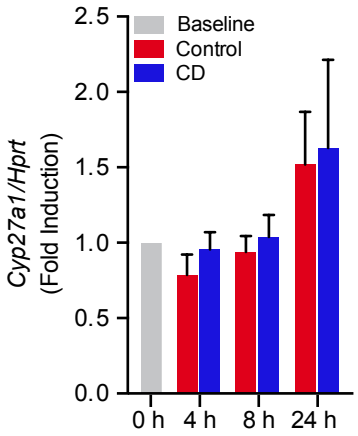


**Fig. S6. CD does not affect *Cyp27a1* expression.** Bone marrow-derived macrophages from WT mice were loaded with 100 µg CC/1x$10^6$ cells over night and then incubated with 10 mM CD or medium control for up to 24 hours. *Cyp27a1* expression calculated relative to the reference gene *Hprt* and presented as fold induction of 0 hour control. Data are shown as mean + s.e.m of four independent experiments.

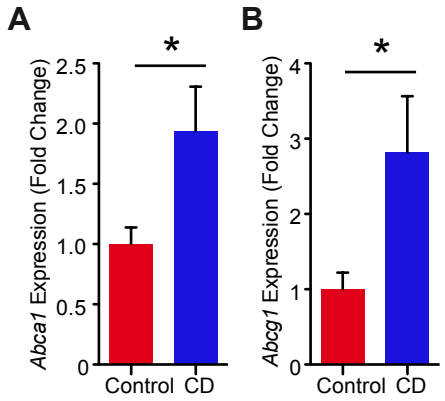


**Fig. S7. CD treatment induces the expression of cholesterol efflux transporters in aortic arches of atherosclerotic mice.** Gene expression of **(A)** *Abca1* and **(B)** *Abcg1* in aortic tissue of ApoE$^{-/-}$ mice after eight weeks of cholesterol-rich diet and concomitant treatment with 2 g CD/ kg body weight or vehicle control twice a week (n=7-8 per group). Data are shown as mean + s.e.m. Control vs. CD, unpaired two-tailed Student's t test; *$p < 0.05$.

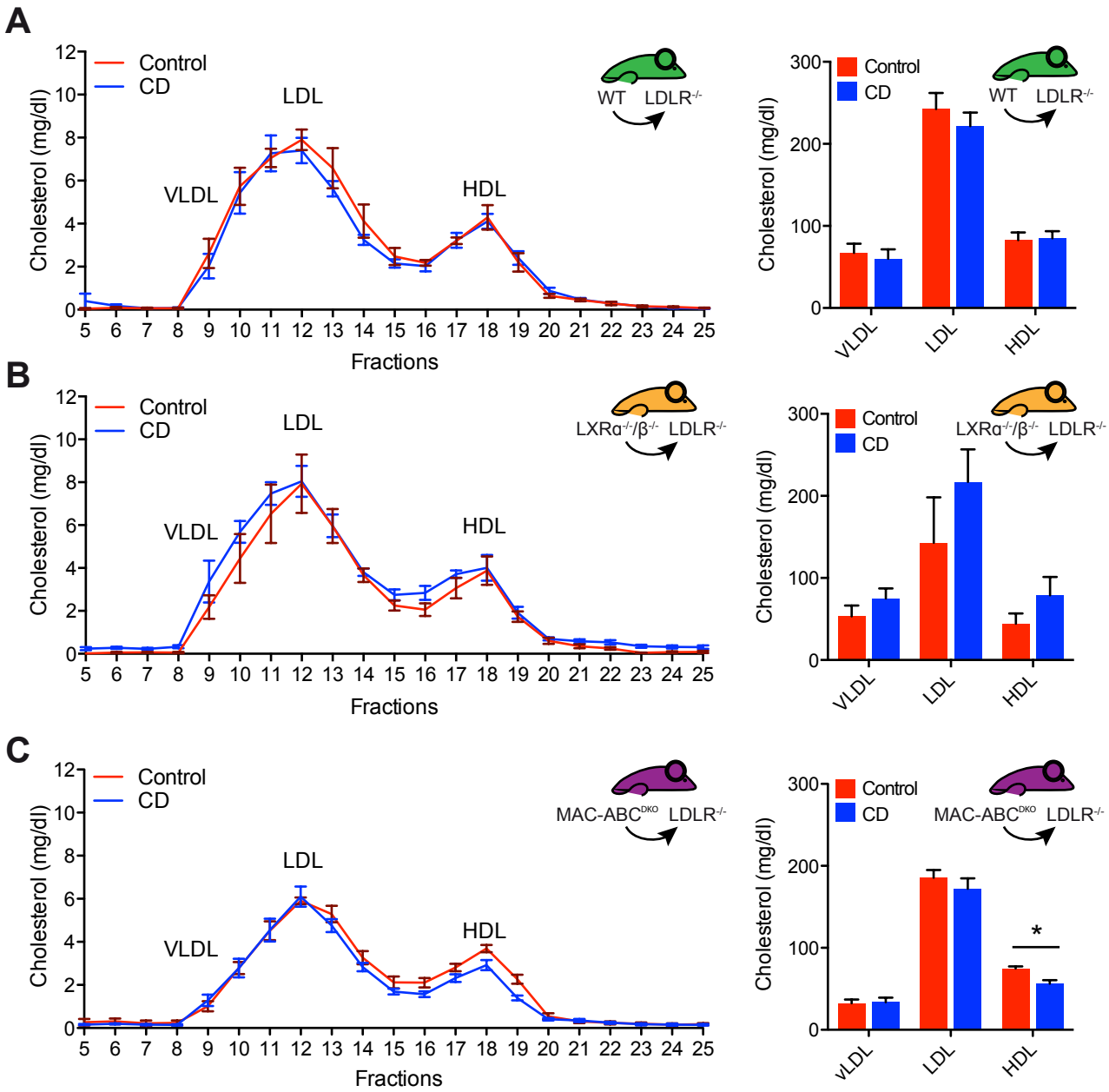


**Fig. S8. CD treatment does not alter murine lipoprotein profiles.** Lipoprotein profiles of LDLR$^{-/-}$ mice transplanted with **(A)** WT, **(B)** LXRα$^{-/-}$β$^{-/-}$, or **(C)** MAC-ABC$^{DKO}$ bone marrow, fed a cholesterol-rich diet for eight weeks and concomitantly treated with 2 g CD/ kg body weight or vehicle control twice a week (n=6-8 per group). Data are shown as mean + s.e.m. or mean +/- s.e.m.

**Table S1. LXR target gene list for GSEA analysis of BMDMs from WT and LXRα$^{-/-}$β$^{-/-}$ mice.** The list contains 533 distinct LXR target genes identified in Heinz *et al. (30)* covered by the Illumina Array.

| LXR target gene names | Accession no. |
|---|---|
| *Abcg1* | NM_009593 |
| *2310035K24Rik* | NM_027129.2 |
| *Col4a3bp* | NM_023420.1 |
| *2310005P05Rik* | NM_026189.2 |
| *Ptpro* | NM_011216.2 |
| *Rgl1* | NM_016846.3 |
| *Psap* | NM_011179.2 |
| *5033414K04Rik* | NM_001003948.1 |
| *Scd1* | NM_009127.3 |
| *Cirbp* | NM_007705.2 |
| *Stx8* | NM_018768.2 |
| *Osgin1* | NM_027950.1 |
| *Acsl3* | NM_028817.2 |
| *1110032E23Rik* | NM_133187.2 |
| *Klf9* | NM_010638.4 |
| *2810439F02Rik* | AK080904 |
| *Fbxo32* | NM_026346.1 |
| *Acly* | NM_134037.2 |
| *Chd9* | NM_177224.1 |
| *Tmem86a* | NM_026436.3 |
| *Sgk1* | NM_011361.1 |
| *Ermp1* | NM_001081213.1 |
| *Slc15a3* | NM_023044.1 |
| *Cd28* | NM_007642.2 |
| *Cpeb2* | NM_175937.2 |
| *Irf8* | NM_008320.3 |
| *Fut8* | NM_016893.4 |
| *Scotin* | NM_025858.1 |
| *Slc1a4* | NM_018861.2 |
| *Sesn1* | NM_001013370.1 |
| *D6Wsu176e* | NM_138587.4 |
| *Sag* | NM_009118.2 |
| *Acp2* | NM_007387.1 |
| *Tlr4* | NM_021297.1 |
| *Tmem120a* | NM_172541.2 |
| *Endod1* | NM_028013.2 |
| *Ccnd3* | NM_007632.2 |
| *Tgfbr2* | AK090393 |
| *Nnat* | AK077465 |
| *Bcar3* | NM_013867.1 |

| | |
|---|---|
| *Fgd2* | NM_013710.3 |
| *Cd63* | NM_007653.1 |
| *2610307O08Rik* | XM_921606.2 |
| *Lrrk1* | NM_146191.3 |
| *Snx27* | NM_029721.1 |
| *Aebp2* | AK045838 |
| *Traf3ip2* | NM_134000.3 |
| *Abca1* | NM_013454.3 |
| *Pdgfb* | NM_011057.2 |
| *Chd2* | NM_001081345.1 |
| *Tatdn2* | NM_001033463.1 |
| *Lpin1* | NM_015763 |
| *1700025G04Rik* | NM_197990.2 |
| *Atp1a1* | NM_144900.1 |
| *Tnfaip2* | NM_009396.1 |
| *6430548M08Rik* | NM_172286 |
| *Dusp6* | NM_026268.2 |
| *Pik3ap1* | NM_031376.2 |
| *Aldh4a1* | NM_175438.3 |
| *Gpx1* | NM_008160.5 |
| *3830408P04Rik* | NM_023647 |
| *Ripk5* | NM_172516.4 |
| *Rheb* | NM_053075.2 |
| *Fam129b* | NM_146119.1 |
| *Mafk* | NM_010757.2 |
| *2810046L04Rik* | NM_173382 |
| *Mylc2b* | NM_023402.1 |
| *Ptgs1* | NM_008969.3 |
| *Txnip* | NM_023719.1 |
| *Hif1a* | NM_010431.1 |
| *Tspan14* | NM_145928.1 |
| *2010107E04Rik* | NM_027360.2 |
| *Ly86* | NM_010745.1 |
| *Irf2* | NM_008391.3 |
| *5430435G22Rik* | NM_145509.2 |
| *A530088I07Rik* | AK080244 |
| *Agpat4* | NM_026644.1 |
| *Tmc6* | NM_145439.1 |
| *Cyth4* | NM_028195.3 |
| *4921513D23Rik* | NM_001081154 |
| *Atp2a2* | NM_009722.2 |
| *Nob1* | NM_026277.1 |
| *Ccdc109b* | NM_025779.2 |
| *9430041J06Rik* | NM_001081045 |
| *Prkcd* | NM_011103.2 |
| *Insr* | AK052187 |
| *Bex6* | NM_001033539.2 |

| | |
|---|---|
| *Slc15a4* | NM_133895.1 |
| *Ptprs* | NM_011218.1 |
| *Tmem17* | NM_153596.1 |
| *Vac14* | NM_146216.2 |
| *Prkar1a* | NM_021880.2 |
| *Uck2* | NM_030724.3 |
| *Sh3yl1* | NM_013709.4 |
| *Erlin2* | NM_153592.1 |
| *Cpsf6* | NM_001013391.1 |
| *Bola3* | NM_175277.2 |
| *Sdc1* | NM_011519.2 |
| *Nrbf2* | NM_001036293.2 |
| *N6amt1* | NM_026366.1 |
| *Mylip* | NM_153789.3 |
| *Bcat1* | NM_007532.3 |
| *Aoah* | NM_012054.2 |
| *Srebf1* | NM_011480.1 |
| *Cdkn2aipnl* | NM_029976.2 |
| *Ak2* | NM_016895.3 |
| *Mdm1* | NM_148922.2 |
| *Adcy7* | NM_007406.1 |
| *Ikbke* | NM_019777.3 |
| *Tnfaip3* | NM_009397.2 |
| *Gng10* | NM_025277.3 |
| *Adrbk1* | NM_130863.1 |
| *Scd2* | NM_009128.1 |
| *5730525O22Rik* | AK017789 |
| *Mtap7* | NM_008635 |
| *Cdk6* | NM_009873.2 |
| *Zzz3* | NM_198416.2 |
| *Nfia* | NM_177176.2 |
| *Maf* | NM_001025577.2 |
| *Rbpj* | NM_009035.4 |
| *B4galt5* | NM_019835.2 |
| *Ccdc45* | NM_177088.2 |
| *Dtnb* | AK083752 |
| *Cd97* | NM_011925.1 |
| *St6gal1* | NM_145933.3 |
| *Pmp22* | NM_008885.2 |
| *Clec2d* | NM_053109.2 |
| *Luzp1* | NM_024452.2 |
| *Grcc10* | NM_013535.1 |
| *S100a6* | NM_011313.2 |
| *Mrpl1* | NM_053158.1 |
| *Ltbp1* | AK054512 |
| *Klhdc4* | NM_145605.1 |
| *Fasn* | NM_007988.3 |

| | |
|---|---|
| *Tmem23* | NM_144792.2 |
| *Nfkb2* | NM_019408.1 |
| *Junb* | NM_008416.1 |
| *Gpr68* | NM_175493.2 |
| *9830002I17Rik* | XM_126365.3 |
| *Spp1* | NM_009263.1 |
| *2700038C09Rik* | NM_025598.1 |
| *Rasgef1b* | NM_181318.4 |
| *Prkcbp1* | NM_027230.3 |
| *Med8* | NM_020000.2 |
| *Usp7* | NM_001003918.2 |
| *Tlr2* | NM_011905.2 |
| *2310040G24Rik* | XM_001480154.1 |
| *Fndc7* | NM_177091.2 |
| *Clstn3* | NM_153508.3 |
| *Slc4a4* | NM_018760.1 |
| *Epb7.2* | NM_013515.1 |
| *Nfyb* | NM_010914.2 |
| *Lrrc33* | NM_146069.4 |
| *Vav3* | NM_020505.2 |
| *Ptafr* | XM_357441.1 |
| *Mdfic* | NM_175088.3 |
| *6330442E10Rik* | NM_178745.3 |
| *Rapgef2* | NM_001099624.1 |
| *Synpr* | NM_028052.3 |
| *Il6ra* | NM_010559.2 |
| *Phlpp* | XM_129968.4 |
| *Reep3* | NM_178606.4 |
| *Uchl4* | NM_033607.1 |
| *Cdk5rap2* | NM_145990.3 |
| *Taf5* | NM_177342.3 |
| *2310045A20Rik* | NM_172710.3 |
| *Papd4* | NM_133905.1 |
| *Pi4kb* | NM_175356.1 |
| *Wnt5a* | NM_009524.2 |
| *Fer1l3* | XM_001480162.1 |
| *Prss2* | NM_009430.1 |
| *Cd9* | NM_007657.2 |
| *Cebpd* | NM_007679.4 |
| *Ralgds* | NM_009058.1 |
| *Entpd1* | NM_009848 |
| *Wsb1* | NM_001042565.2 |
| *Snx29* | NM_028964.3 |
| *Nfe2l2* | NM_010902.3 |
| *Gas7* | NM_008088.1 |
| *Scd3* | NM_024450.2 |
| *Mrpl33* | NM_025796.2 |

| | |
|---|---|
| *Socs3* | NM_007707.2 |
| *Gabpb2* | NM_029885.1 |
| *AB124611* | NM_206536.1 |
| *Dtd1* | NM_025314.1 |
| *Lox* | NM_010728.1 |
| *6330503K22Rik* | NM_182995.1 |
| *Cnot2* | NM_028082.1 |
| *Icam2* | NM_010494.1 |
| *Cxcl4* | NM_019932.2 |
| *Ttpal* | NM_029512.2 |
| *Plekho2* | NM_153119.2 |
| *Dppa3* | NM_139218.1 |
| *Asph* | NM_133723.2 |
| *Stx7* | NM_016797.4 |
| *Stard3nl* | NM_024270.2 |
| *Eya3* | NM_010166.2 |
| *Prrc1* | NM_028447.2 |
| *Fhl3* | AF114382 |
| *D930001I22Rik* | NM_173397 |
| *2210010L05Rik* | NM_133829.1 |
| *Syne2* | NM_001005510.2 |
| *Abr* | NM_198894.1 |
| *Creg1* | NM_011804.2 |
| *Fcgr1* | NM_010186.4 |
| *Il17rd* | NM_134437.1 |
| *Cdc2l5* | NM_001081058.1 |
| *Dpp3* | NM_133803.1 |
| *Rhoc* | NM_007484.1 |
| *Unc5b* | NM_029770.2 |
| *5830415L20Rik* | NM_001042501.1 |
| *Arhgef10l* | NM_172415.2 |
| *Atp5g3* | NM_175015.2 |
| *Adk* | NM_134079.1 |
| *Timm13* | NM_013895.2 |
| *Adss* | NM_007422.2 |
| *Zc3h11a* | NM_144530.5 |
| *Prx* | NM_198048.1 |
| *Ngrn* | NM_031375.3 |
| *Tmem120b* | NM_001039723.2 |
| *Prkag2* | NM_145401.1 |
| *Ppp3r1* | NM_024459.2 |
| *Atp13a3* | XM_001480958.1 |
| *Eif2ak4* | AK077199 |
| *Pfkfb2* | NM_008825.3 |
| *Acsl4* | NM_001033600.1 |
| *Zubr1* | XM_001479450.1 |
| *2310043N10Rik* | NR_003513.2 |

| | |
|---|---|
| *Lass6* | NM_172856.3 |
| *Coro6* | NM_139128.1 |
| *Fkbp3* | NM_013902.4 |
| *Ankrd55* | NM_029898.2 |
| *Ddx50* | NM_053183.1 |
| *Laptm4a* | NM_008640.2 |
| *Lrrc28* | NM_175124.4 |
| *Rara* | NM_009024.2 |
| *Notch2* | NM_010928.1 |
| *Rpl31* | NM_053257.1 |
| *5031425E22Rik* | XM_149592.1 |
| *Atp8b4* | XM_141343 |
| *H2afx* | NM_010436.2 |
| *Emg1* | NM_013536.1 |
| *Ssfa2* | NM_080558 |
| *2610204M08Rik* | NM_198411.2 |
| *Akr1a4* | NM_021473.2 |
| *Art3* | NM_181728.1 |
| *E030010A14Rik* | NM_183160.3 |
| *Galnt9* | NM_198306.1 |
| *Abca17* | NM_001031621.1 |
| *Actn1* | NM_134156.1 |
| *Tacc1* | NM_199323.2 |
| *Zc3h12a* | NM_153159.1 |
| *Muc1* | NM_013605.1 |
| *Cnpy3* | NM_028065.2 |
| *Hivep2* | NM_010437.2 |
| *Cc2d1b* | NM_177045.2 |
| *Eif4a2* | NM_013506 |
| *Cmah* | NM_007717.1 |
| *Zeb2* | NM_015753.3 |
| *Cux1* | NM_009986.3 |
| *Npm3-ps1* | NR_002702.1 |
| *C5ar1* | NM_007577.3 |
| *Adap2* | NM_172133.1 |
| *Smap2* | NM_133716.2 |
| *Tle4* | NM_011600.2 |
| *Col17a1* | NM_007732.1 |
| *Hoxa1* | NM_010449.3 |
| *AI836003* | NM_177716.2 |
| *Hal* | NM_010401.3 |
| *Usp6nl* | NM_181399.3 |
| *Olfr726* | NM_146316 |
| *Wdfy3* | NM_172882 |
| *Myo3b* | XM_194023.1 |
| *Erh* | NM_007951.1 |
| *Rps19bp1* | NM_175109.3 |

| | |
|---|---|
| *Btg2* | NM_007570.2 |
| *Dcbld2* | NM_028523.3 |
| *Ttc9* | NM_001033149.2 |
| *Mrpl2* | NM_025302.3 |
| *Birc6* | AK086619 |
| *Itgb1* | NM_010578.1 |
| *Nup160* | NM_021512.2 |
| *Mnt* | NM_010813.2 |
| *Emp1* | NM_010128.4 |
| *Bcl7b* | NM_009745.1 |
| *Nfatc4* | NM_023699.2 |
| *Creb3l2* | NM_178661.3 |
| *Gtf2e1* | NM_028812.3 |
| *Ado* | NM_001005419.1 |
| *Atp5l* | NM_013795.4 |
| *3110003A17Rik* | NM_028440.1 |
| *1700017N19Rik* | XM_487140 |
| *Cltc* | NM_001003908 |
| *Cdca3* | NM_013538.4 |
| *Dhx35* | NM_145742.1 |
| *Aldh9a1* | NM_019993.3 |
| *Sall4* | NM_175303.3 |
| *Tiprl* | NM_145513.3 |
| *Bbc3* | NM_133234.1 |
| *Jph1* | NM_020604.1 |
| *Zfand3* | NM_148926.2 |
| *Gdi2* | NM_008112.4 |
| *Tex14* | NM_031386.1 |
| *Nuak1* | NM_001004363.1 |
| *Rffl* | NM_001007465.1 |
| *Slc5a3* | NM_017391.2 |
| *Cntnap5a* | NM_001077425.1 |
| *Egr3* | NM_018781 |
| *Gpatch4* | NM_025663.2 |
| *Ggnbp1* | NM_027544.1 |
| *Il20ra* | NM_172786.1 |
| *2310005N03Rik* | NM_025511.2 |
| *Opn5* | NM_181753.2 |
| *8430432M10Rik* | NM_176831.2 |
| *Gm826* | NM_001033411.1 |
| *Lyzl4* | NM_026915.2 |
| *1700012B15Rik* | NM_028796 |
| *Col22a1* | XM_907370.3 |
| *H2-Q1* | NM_010390.2 |
| *Prnpip1* | NM_080469.2 |
| *Mgat5* | NM_145128.3 |
| *S1pr1* | NM_007901.4 |

| | |
|---|---|
| *Lass2* | NM_029789.1 |
| *Alad* | NM_008525.3 |
| *Mppe1* | NM_172630.1 |
| *Zc3h14* | NM_029334.1 |
| *Ifnar2* | NM_010509.1 |
| *Tmem119* | NM_146162.1 |
| *St6galnac6* | NM_001025311.1 |
| *Sepn1* | NM_029100.2 |
| *Veph1* | NM_145820.1 |
| *Dirc2* | NM_153550.3 |
| *Gucy2g* | NM_001081076.1 |
| *Tsen2* | NM_199033.1 |
| *C130026I21Rik* | NM_175219.3 |
| *Gsx1* | NM_008178.2 |
| *Slc7a1* | NM_007513.3 |
| *Txndc11* | NM_134105.2 |
| *Plce1* | NM_019588.2 |
| *1700112H15Rik* | XM_149010.2 |
| *Tmem41b* | NM_153525.5 |
| *Cdca1* | NM_023284.1 |
| *Gm71* | NM_001033236.2 |
| *AI427809* | NM_001033454.1 |
| *Grk5* | NM_018869.2 |
| *B3galnt1* | NM_020026.2 |
| *Gda* | AK044078 |
| *Cps1* | NM_001080809.1 |
| *Esr1* | NM_007956.4 |
| *5430405G24Rik* | XM_152907.3 |
| *Hnt* | NM_172290.3 |
| *March7* | NM_020575.2 |
| *Nomo1* | NM_153057.3 |
| *Sfpi1* | NM_011355.1 |
| *Tm7sf3* | NM_026281.2 |
| *1600014C10Rik* | NM_028166.3 |
| *Brms1* | NM_134155.1 |
| *Hells* | NM_008234.3 |
| *Fndc3b* | NM_173182.1 |
| *Axl* | NM_009465.3 |
| *2810474O19Rik* | NM_026054.2 |
| *6530418L21Rik* | NM_175398.3 |
| *Phtf2* | NM_172992.2 |
| *Leprel2* | NM_013534.4 |
| *Cenpn* | NM_028131.3 |
| *Tdrd7* | NM_146142.1 |
| *Arid1a* | NM_033566.1 |
| *Dusp14* | NM_019819.3 |
| *Cic* | NM_027882.2 |

| | |
|---|---|
| *Ifnab* | NM_008336.2 |
| *1700027L20Rik* | XM_906114.3 |
| *Cd19* | NM_009844.2 |
| *Sf1* | NM_011750.1 |
| *1700011E24Rik* | XM_128789.5 |
| *Terf2ip* | NM_020584.1 |
| *Ogg1* | NM_010957.3 |
| *Tmem69* | NM_177670.3 |
| *Casc1* | NM_177222.3 |
| *Lpl* | NM_008509.2 |
| *Gm572* | NM_001085505.1 |
| *Itpkc* | NM_181593.2 |
| *Crat* | NM_007760.3 |
| *1700019M22Rik* | NM_027076.2 |
| *Akna* | NM_001045514.1 |
| *Fam176b* | NM_172145.3 |
| *Itpr2* | NM_010586.1 |
| *Slc7a14* | NM_172861.2 |
| *Bcl2l1* | NM_009743.4 |
| *BC006965* | NM_146031 |
| *Cryga* | NM_007774.3 |
| *Fli1* | NM_008026.4 |
| *Selk* | NM_019979.1 |
| *Clca5* | NM_178697.4 |
| *Osbpl9* | NM_173350.1 |
| *Lpcat3* | NM_145130.1 |
| *1500035H01Rik* | NM_023831.3 |
| *Zfp644* | NM_026856.2 |
| *2310033K02Rik* | NM_001080708.1 |
| *B3gat1* | NM_029792.1 |
| *Nubpl* | NM_029760.1 |
| *March8* | NM_027920.4 |
| *Sergef* | NM_013789.1 |
| *Slc30a6* | NM_144798.4 |
| *3110023E09Rik* | AK014071 |
| *Foxc1* | NM_008592.2 |
| *Cln6* | NM_001033175.1 |
| *D4Ertd196e* | XM_975887.1 |
| *1810019J16Rik* | NM_001083916.1 |
| *Ube2i* | NM_011665.3 |
| *Clec4d* | NM_010819.3 |
| *A430090L17Rik* | NM_177004 |
| *Sspn* | NM_010656.2 |
| *Pim1* | NM_008842.3 |
| *Tatdn1* | NM_175151.2 |
| *Uqcrc2* | NM_025899.2 |
| *Lrp1* | NM_008512.2 |

| | |
|---|---|
| *Tnrc4* | NM_172434.2 |
| *Maz* | XM_133827.2 |
| *Etv6* | NM_007961.3 |
| *Arl6ip6* | NM_022989.2 |
| *Atp8b2* | NM_001081182.1 |
| *Cetn1* | NM_007593.5 |
| *Iqch* | XM_981814.1 |
| *Spink10* | NM_177829.3 |
| *C230095G01Rik* | NM_178768.3 |
| *Grin2b* | NM_008171.3 |
| *Mmp9* | NM_013599.2 |
| *Hsd11b1* | NM_008288.1 |
| *Wipf2* | NM_197940.1 |
| *Ncf4* | NM_008677.1 |
| *4932443I19Rik* | XM_980156.1 |
| *Dr1* | NM_026106.4 |
| *C730024G19Rik* | XM_921354.2 |
| *Tmc1* | NM_028953.2 |
| *Eps8* | NM_007945.2 |
| *Efna1* | NM_010107.3 |
| *Ptp4a2* | NM_008974.2 |
| *Pacrgl* | NM_025755.3 |
| *4932425I24Rik* | NM_001081025.1 |
| *Slc6a14* | NM_020049.3 |
| *Arf2* | NM_007477.4 |
| *Prr13* | NM_025385.2 |
| *4930543E12Rik* | XM_922816 |
| *Edem1* | NM_138677.2 |
| *D1Ertd471e* | NM_001164528 |
| *Nsl1* | NM_198654.2 |
| *Rnf186* | NM_025786.2 |
| *Ptchd3* | XM_109751.6 |
| *Smg7* | NM_001005507.1 |
| *Wdr36* | NM_144863.3 |
| *BC017158* | NM_145590.1 |
| *Gapdh* | NM_008084.2 |
| *Rps20* | NM_026147 |
| *Chmp4b* | NM_029362.3 |
| *2310028O11Rik* | XM_901483.3 |
| *Dip2c* | NM_001081426.1 |
| *Igsf3* | NM_207205.1 |
| *Pon1* | NM_011134.2 |
| *OTTMUSG00000000997* | NM_001037932.1 |
| *Fcer1g* | NM_010185.2 |
| *Olfr951* | NM_001011812.1 |
| *Cct5* | NM_007637.2 |
| *Rps27a* | NM_001033865.1 |

| | |
|---|---|
| *4930522O17Rik* | XM_898933.3 |
| *Diap2* | NM_017398.2 |
| *Fmnl1* | NM_019679.2 |
| *1200011M11Rik* | NM_024262.1 |
| *Bckdhb* | NM_199195.1 |
| *Htr6* | NM_021358.1 |
| *Galnt4* | NM_015737.3 |
| *Olfr586* | NM_147111.1 |
| *Scnn1a* | NM_011324.1 |
| *Dpp10* | NM_199021.2 |
| *Scg5* | NM_009162.3 |
| *Exoc2* | NM_025588.2 |
| *Elovl5* | NM_134255.2 |
| *Trcg1* | NM_001014398.1 |
| *Dlx1as* | NR_002854.1 |
| *Tmem16b* | NM_153589.1 |
| *Zfp364* | NM_026406.2 |
| *Zc3h6* | NM_178404.2 |
| *Grm4* | NM_001013385.1 |
| *Ppp1r9b* | NM_172261.2 |
| *Gh* | NM_008117.2 |
| *Phospho1* | NM_153104.2 |
| *4930546C10Rik* | XM_484744 |
| *Sh3bgrl3* | NM_080559.1 |
| *Zmat5* | NM_026015.2 |
| *Cngb3* | NM_013927.2 |
| *Hip1* | NM_146001 |
| *2310011J03Rik* | NM_025521.3 |
| *Rassf8* | NM_027760.2 |
| *Arl4d* | NM_031160.1 |
| *Morn4* | NM_198108.2 |
| *Mef2d* | NM_133665.3 |
| *Mgst3* | NM_025569.1 |
| *Ctsd* | NM_009983.2 |
| *Gm528* | XM_986482.1 |
| *Bms1* | NM_194339.1 |
| *Slc13a4* | NM_172892.1 |
| *Bard1* | NM_007525.2 |
| *Cd5l* | NM_009690.1 |
| *Npffr1* | XM_905368.1 |
| *Pltp* | NM_011125.2 |
| *2610209M04Rik* | NM_025665.1 |
| *1700010C24Rik* | NM_027401.2 |
| *Ctss* | NM_021281.1 |
| *Il6* | NM_031168.1 |
| *Ubash3b* | NM_176860.5 |
| *Pgs1* | NM_133757.2 |

| | |
|---|---|
| *Ror1* | NM_013845.4 |
| *Cyp26b1* | NM_175475.2 |
| *Psma6* | NM_011968.2 |
| *Kpna2* | NM_010655.3 |
| *Myo16* | NM_001081397.1 |
| *Mllt6* | NM_139311.2 |
| *S100a7a* | NM_199422.1 |
| *Sec22b* | NM_011342.2 |
| *Gltp* | NM_019821.2 |
| *Ssbp4* | NM_133772.1 |
| *1600002D24Rik* | XM_001473403.1 |
| *Gad2* | NM_008078.1 |
| *Oxa1l* | NM_026936.3 |
| *1600014C23Rik* | XM_128667.1 |
| *Commd4* | NM_025417.1 |
| *Frrs1* | NM_009146.1 |
| *4933402G07Rik* | AK016617 |
| *Chsy1* | NM_001081163.1 |
| *Mnd1* | NM_029797.1 |
| *Setdb1* | NM_018877.2 |
| *Spry4* | NM_011898.2 |
| *Mtx2* | NM_016804.2 |
| *Prl4a1* | NM_011165.3 |

**Table S2. LXR target gene list for GSEA analysis of human atherosclerotic plaques.** The list contains direct LXR target genes identified in Pehkonen *et al. (54)* covered by the nCounter GX Human Immunology Kit v2 (Nanostring Technologies) and the 30 additional genes in table S3.

| **LXR target gene names** | **Accession no.** |
|---|---|
| *ABCA1* | NM_005502.2 |
| *ABCG1* | NM_207174.1 |
| *ABL1* | NM_005157.3 |
| *BAX* | NM_138761.3 |
| *BID* | NM_001196.2 |
| *BIRC2* | NM_001166.3 |
| *CCR6* | NM_031409.2 |
| *CD276* | NM_001024736.1 |
| *CD44* | NM_001001392.1 |
| *CD58* | NM_001779.2 |
| *CD82* | NM_002231.3 |
| *CEBPB* | NM_005194.2 |
| *DUSP4* | NM_057158.2 |

| | |
|---|---|
| *EGR1* | NM_001964.2 |
| *ETS1* | NM_005238.3 |
| *FADD* | NM_003824.2 |
| *GNLY* | NM_006433.2 |
| *HLA-DRB1* | NM_002124.2 |
| *HSP90AA1* | NM_001017963.2 |
| *ICAM3* | NM_002162.3 |
| *IL1RN* | NM_000577.3 |
| *IRF5* | NM_002200.3 |
| *ITGAX* | NM_000887.3 |
| *LILRB3* | NM_006864.2 |
| *MCL1* | NM_021960.3 |
| *MIF* | NM_002415.1 |
| *NFATC3* | NM_004555.2 |
| *NLRP3* | NM_001079821.2 |
| *NR1H3* | NM_005693.2 |
| *PRDM1* | NM_001198.3 |
| *PRKCD* | NM_006254.3 |
| *PSMB8* | NM_004159.4 |
| *PTGER4* | NM_000958.2 |
| *RPL19* | NM_000981.3 |
| *S100A8* | NM_002964.3 |
| *S100A9* | NM_002965.2 |
| *SDHA* | NM_004168.1 |
| *SMAD5* | NM_005903.5 |
| *STAT3* | NM_139276.2 |
| *TGFBR2* | NM_001024847.1 |
| *TNF* | NM_000594.2 |
| *TRAF3* | NM_145725.1 |
| *TUBB* | NM_178014.2 |
| *XBP1* | NM_005080.2 |

**Table S3. List of additional metabolic and regulatory genes (nCounter Panel Plus).** The nCounter GX Human Immunology Kit v2 (Nanostring Technologies) was extended by probes for 30 additional genes.

| **Gene names** | **Accession no.** |
|---|---|
| *ABCA1* | NM_005502.2 |
| *ABCG1* | NM_207174.1 |
| *ACAT1* | NM_000019.2 |

| | |
|---|---|
| *APOA1* | NM_000039.1 |
| *APOE* | NM_000041.2 |
| *BIRC2* | NM_001166.3 |
| *BIRC3* | NM_182962.1 |
| *CASP5* | NM_004347.1 |
| *CETP* | NM_000078.2 |
| *CYP27A1* | NM_000784.3 |
| *CYP7A1* | NM_000780.3 |
| *HSP90AA1* | NM_001017963.2 |
| *HSP90AB1* | NM_007355.2 |
| *HSP90B1* | NM_003299.1 |
| *LPL* | NM_000237.2 |
| *MAP3K7* | NM_145333.1 |
| *NFKBIB* | NM_002503.3 |
| *NLRC4* | NM_021209.3 |
| *NLRP1* | NM_033004.2 |
| *NR1H2* | NM_007121.4 |
| *NR1H3* | NM_005693.2 |
| *PLTP* | NM_006227.2 |
| *PPARD* | NM_006238.4 |
| *PSTPIP1* | NM_003978.3 |
| *PYDC1* | NM_152901.2 |
| *RIPK2* | NM_003821.5 |
| *SCARB1* | NM_005505.3 |
| *SLC2A4* | NM_001042.2 |
| *SREBF1* | NM_001005291.1 |
| *SUGT1* | NM_006704.3 |

**Table S4. Original data for all figures.** Microsoft Excel spreadsheet including all original data and exact p-values for significant results.